POLITECNICO
MILANO 1863

SCUOLA DI INGEGNERIA INDUSTRIALE
E DELL'INFORMAZIONE

# A Preliminary Techno-Economic Evaluation of Airborne Wind Energy for Offshore Applications in Italy

Tesi di Laurea Magistrale in
Energy Engineering - Ingegneria Energetica

Author: **Francesca Neri, Umberto Nobile**

Student ID: 227149, 260443
Advisor: Prof. Alessandro Croce
Academic Year: 2024-2025

# Abstract

The decarbonization pathway undertaken by Italy and the European Union toward the 2030 climate targets requires a rapid acceleration in the deployment of innovative renewable energy technologies. Among the emerging solutions, Airborne Wind Energy (AWE) stands out as a promising yet still pre-commercial concept capable of exploiting high altitude winds, which are generally stronger and more persistent than those accessed by conventional turbines. Thanks to lightweight airborne structures and minimal spatial footprint, AWE systems offer the potential for flexible renewable generation with reduced environmental impact.

Although AWE remains at an intermediate technology readiness level and faces challenges related to automation, reliability and certification, ongoing developments indicate a clear trajectory toward multi-megawatt devices and more complex offshore applications.

In this context, the main objective of this thesis is to provide a preliminary techno-economic assessment of offshore AWE deployment in Italian maritime areas.

The analysis addresses two complementary aspects: first, the characterization of high-altitude offshore winds through a comparison between ERA5 and CERRA reanalyses, and the estimation of large-scale theoretical offshore AWE potential; then, an evaluation of cost competitiveness through the computation of the Levelized Cost of Energy (LCoE).

The analysis confirmed that Italy has an enormous theoretical offshore AWE potential, capable of exceeding the country's annual electricity consumption. The results also showed that, although the current LCoE reflects the pre commercial nature of the technology and is dominated by offshore infrastructure costs, the economic gap with mature technologies can be significantly reduced through design optimization and targeted incentive policies.

In conclusion, this study validates offshore AWE as an energy option with high theoretical potential for Italy. The analysis provides a consistent methodological foundation and outlines future research directions necessary to improve both the technological efficiency of AWE systems and the accuracy of analyses and forecasts of key data such as the Levelized Cost of Energy. The results offer essential estimates to support future research

and preliminary investment evaluations, accelerating the integration of AWE into Italy's future energy portfolio.

**Keywords:** Airborne Wind Energy, Offshore wind, Techno-economic assessment, LCoE, Reanalysis datasets, Annaul Energy Production.

# Abstract in lingua italiana

Il percorso di decarbonizzazione intrapreso dall'Italia e dall'Unione Europea verso gli obiettivi climatici del 2030 richiede una rapida accelerazione nella diffusione di tecnologie innovative per le energie rinnovabili. Tra le soluzioni emergenti, i sistemi Airborne Wind Energy (AWE) si distingue come un concetto promettente ma ancora pre-commerciale, in grado di sfruttare i venti d'alta quota, generalmente più forti e persistenti di quelli a cui accedono le turbine convenzionali. Grazie a strutture aeree leggere e ad un ingombro spaziale minimo, i sistemi AWE offrono il potenziale per una generazione flessibile di energia rinnovabile con un impatto ambientale ridotto.

Sebbene i sistemi AWE rimangano a un livello intermedio di conoscenza tecnologica e debbano affrontare sfide legate all'automazione, all'affidabilità e alla certificazione, gli sviluppi in corso indicano una chiara traiettoria verso dispositivi multi-megawatt e applicazioni offshore più complesse.

In questo contesto, l'obiettivo principale di questa tesi è quello di fornire una valutazione tecnico-economica preliminare dell'impiego di AWE offshore nelle aree marittime italiane.

L'analisi affronta due aspetti complementari: in primo luogo, la caratterizzazione dei venti offshore ad alta quota attraverso un confronto tra le rianalisi ERA5 e CERRA e la stima del potenziale teorico di AWE offshore su larga scala; in seguito, una valutazione della competitività dei costi attraverso il calcolo del costo livellato dell'energia (LCoE).

L'analisi ha confermato che l'Italia ha un enorme potenziale teorico per i sistemi AWE offshore, in grado di superare il consumo annuo di elettricità del Paese. I risultati hanno inoltre mostrato che, sebbene l'attuale LCoE rifletta la natura precommerciale della tecnologia e sia dominato dai costi delle infrastrutture offshore, il divario economico con le tecnologie mature può essere significativamente ridotto attraverso l'ottimizzazione della progettazione e politiche di incentivi mirate.

In conclusione, questo studio convalida l'AWE offshore come opzione energetica ad alto potenziale teorico per l'Italia. L'analisi fornisce una base metodologica coerente e delinea le future direzioni di ricerca necessarie per migliorare sia l'efficienza tecnologica dei sis-

temi AWE, sia l'accuratezza delle analisi e delle previsioni di dati chiave come il costo dell'energia. I risultati offrono stime essenziali a supporto della ricerca futura e delle valutazioni preliminari degli investimenti, accelerando l'integrazione dei sistemi AWE nel futuro portafoglio energetico italiano.

**Parole chiave:** Airborne Wind Energy, Eolico Offshore, Valutazione Tecnico-Economica, LCoE, Dati di Rianalisi, Produzione Energetica Annuale.

# Contents

# 1 Introduction

## 1.1 Energy scenario

In recent years, the climate crisis has become one of the most pressing issues on the global political and scientific agenda. The intensification of extreme weather events and record breaking temperatures have underscored its urgency: in July 2024, the global mean surface temperature surpassed 17 °C, marking the highest value ever recorded [32]. These developments have reinforced the collective awareness of the need for immediate, coordinated action towards the objectives of the Paris Agreement, which aims to limit global warming to 1.5 °C and accelerate the global energy transition through enhanced climate finance and a substantial increase in renewable capacity by 2030 [32].

Among the main challenges we find the need to decarbonise the sectors that most pollute and the need to guarantee the security and accessibility of energy supplies. Historically, energy consumption has been the main source of greenhouse gas emissions, representing approximately 80% of overall emissions in Italy in 2022 [1].

According to the Energy Transition Commission, a transformation of the energy system is necessary, coupling large scale renewable deployment with improvements in efficiency, storage and grid flexibility to achive low carbon growth [16]. In this context, the transition process inevitably passes through the decarbonization of the energy sector with the use of renewable sources, such as solar and wind, among others, whose generation costs are continuously decreasing [10].

At the international level, the European Union has defined targets for this transition, setting a 55 % reduction in greenhouse gas emissions by 2030 and achieving carbon neutrality by 2050. In this scenario, in Italy, through the Piano Nazionale Integrato per l'Energia e il Clima (PNIEC), a massive increase in installed renewables capacity is expected, reaching almost 80 installed GW of solar and about 28 GW of installed wind capacity [14].

The Bank of Italy analysis shows an acceleration of renewable plant installations from 2022 which is however still insufficient to meet the PNIEC targets. Hydroelectric was

joined first by wind power plants and since 2008 by photovoltaic plants, supported by incentives from the Energy Account. Wind development affected the South of Italy almost exclusively, while the growth profile of photovoltaics was similar between the Centre North and the South [1].

Beyond the European context, COP29 showed that reaching these targets will take more than national commitment, it will need global coordination of carbon markets and at least 300 billion USD a year by 2035 to help developing countries with mitigation and adaptation [32]. This underlines a shared understanding that the energy transition should balance environmental goals with social and economic stability.

In pursuing the goal of full decarbonisation and an energy system based largely on renewables, it is crucial not to limit ourselves to mature wind technologies, but to explore innovative solutions such as Airborne Wind Energy (AWE) [30]. Those systems have the potential to unlock untapped wind resources and contribute to the stability of the electricity system [30].

Airborne Wind Energy systems exploit higher altitude winds by using tethered, autonomous flying devices, such as kites or wings, to harness wind power at altitudes inaccessible to conventional wind turbines. This technology aims to tap into stronger, steadier winds found far above the ground, which can significantly increase energy generation, using less material and potentially reducing capital costs and environmental impact compared to traditional wind farms [3, 30]. AWE system operating up to 500 m above ground can access wind power densities up to twice those available at 100 m, which is the typical hub height of conventional wind turbines and so improving base load capability [3].

However, AWE systerms are still at a pre-commercial stage, requiring further research on regulation and techno-econominc feasibility before large scale deployment [29].

## 1.2 Introduction to Airborne Wind Energy

Airborne Wind Energy represents a radical variance from conventional wind energy systems, differing substantially in its operational principles, design and lifecycle stages. This new approach began to emerge theoretically around 1980, but it is only over the last decade that significant interest and investment in the field have substantially increased [31]. As previously mentioned, AWE harvest kinetic energy from atmospheric flows by using tethered flying devices, typically kites or wings, converting kinetic energy of the wind into electricity. Differently from traditional technologies, it can exploit wind resources at considerably higher altitudes, where the wind is typically stronger, steadier and less affected by surface turbulence than at conventional turbine hub heights. Operational altitudes for AWE systems generally range from about 100 m up to 500 m above ground level, although many of the early studies estimate the wind speed profile up to the height of the jet stream ( 10 km) [31]. These systems can autonomously adjust their flight altitude to track the layer of maximum wind speed, ensuring a more stable and continuous power output over time compared with traditional ground-based wind turbines.
This fundamental differences leads to several distinctive advantages, particularly in terms of material efficiency, flexibility of deployment and potential cost competitiveness.

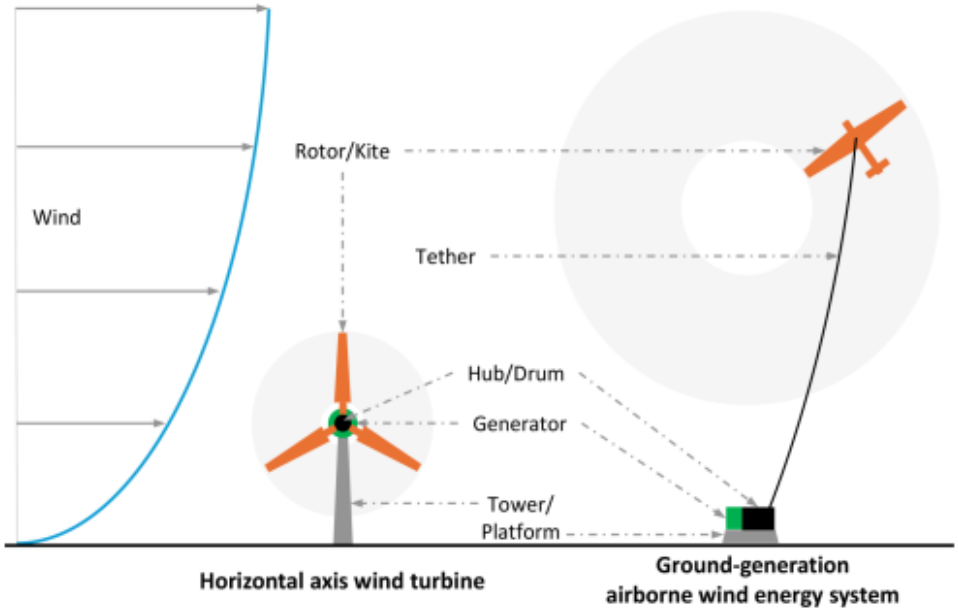


Figure 1.1: Analogy between the components of a horizontal axis wind turbine and a ground-generation Airborne Wind Energy system [12].

From a structural perspective, AWE systems drastically reduce material requirements compared to tower based wind turbines. The absence of a heavy support tower and

massive foundation results in an estimated 70–80% reduction in structural mass [31]. This not only lowers raw material and manufacturing costs, but also simplifies logistics, transport and decommissioning operations. As a result, the embodied energy and carbon footprint per installed kilowatt are significantly reduced, leading to a potentially lower LCoE and improved sustainability indicators across the system's lifecycle.

Another key advantage lies in the flexibility of siting and deployment. Unlike traditional wind systems, which require stable soil and extensive civil works, AWE systems can be installed in areas previously unsuitable for turbines installation, including deep offshore sites, mountainous terrain or isolated regions. Their modular nature and reduced physical footprint allow for rapid installation and relocation, facilitating hybrid configurations with other renewable technologies and enabling decentralized power generation in off-grid contexts. This adaptability expands the geographical scope of wind energy exploitation, particularly for countries with limited shallow offshore areas such as Italy. However, the potential environmental and social impacts and acceptance is still a critical question [15].

In terms of economics, AWE shows strong potential for cost competitiveness. If current prototypes can evolve into multi-megawatt units with optimized power density and short tether configurations, AWE could achieve or even surpass the cost-effectiveness of modern offshore turbines [31]. Lower capital expenditure, simplified maintenance and scalable system architectures may translate into LCoE values below those of conventional wind, especially in regions characterized by high altitude wind resources and limited infrastructure. Moreover, AWE's ability to dynamically adapt to varying wind profiles can result in smoother power generation and a higher effective capacity factor over time [13].

Despite these promising advantages, AWE remains at an early to intermediate stage of technological readiness (Technology Readiness Level, TRL 4–6) [31]. Significant challenges still hinder full scale commercialization. Key challenges include achieving reliable flight automation, fully autonomous takeoff and landing and ensuring the long-term durability of tethers and wings under cyclic loads. The lack of long-term field data also limits the validation of performance models, particularly regarding energy yield stability and maintenance costs.

The current diversity of design concepts within the AWE sector, ranging from soft kites to rigid-wing gliders and from ground-generation to onboard-generation systems, reflects the ongoing experimental nature of this field. This technological heterogeneity, while indicative of strong innovation, also highlights the absence of a dominant design paradigm, confirming that AWE is still in a phase of convergence toward a mature industrial archetype. Table 1.1 and the following paragraphs summarizes the main characteristics and classifi-

cation parameters of the different AWE system typologies [20].

| Concept Attribute | Variants |
|---|---|
| Electrical generation location | In-flight; ground-based fixed; ground-based mobile; other |
| Flight path | Stationary; in tether direction; crosswind with unidirectional rotation; crosswind with bidirectional rotation; other |
| Wing structure | Soft single layer; soft ram-air multicell; soft with inflatable support; soft with nonlinear elastic reinforcement; semirigid; segmented rigid; rigid; multiwing; other |
| Takeoff | Vertical; horizontal; using main aerodynamic system; using embedded ancillary aerodynamic system; centrifugal; catapult; lift system; support system; fan; other |
| Landing | Vertical; horizontal; using main aerodynamic system; using embedded auxiliary aerodynamic system; other |
| Flight region | Low (up to 300 m); medium (300–600 m); high (above 600 m); combined; other |
| Control | Active control surfaces (elevator, elevon, flap, wing deformation); tension control; partly passive; other |
| Energy-conversion stages | Direct generation; mechanical; hydraulic; other |
| Tether topology | Single; bridle; dual; multiple; other |
| Kite topology | Single; twin; rotor; staggered; combined (identical or varied); multiple; networked architectures; other |
| Farm integration | Independent unit; staggered height levels; farm control; other |
| Reference | Fixed; moving; single; multiple; absolute; relative; other |
| Other attributes | Known; to be defined; other |

Table 1.1: Concept attributes and variants of Airborne Wind Energy systems [20].

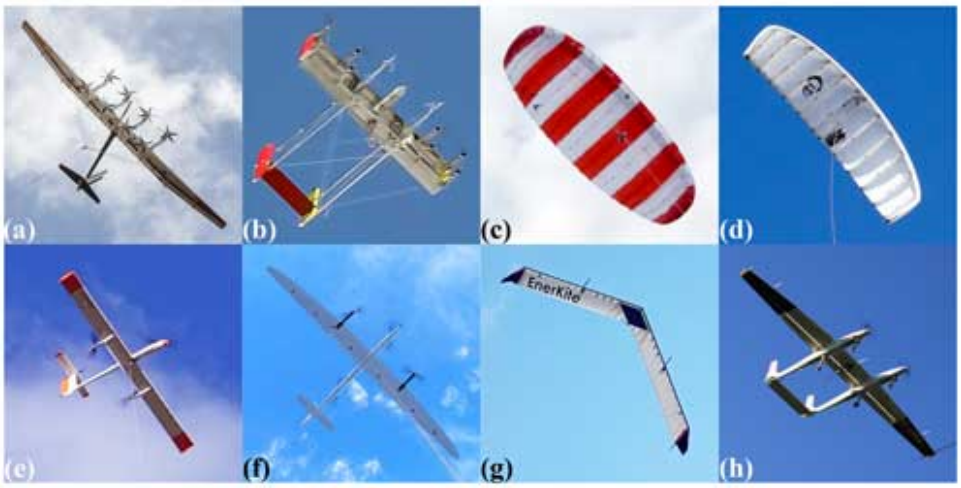


Figure 1.2: AWE system prototypes currently under development [22].

.

### 1.2.1 Power conversion mechanism

Airborne Wind Energy systems are typically composed of a ground system and at least one aircraft, connected mechanically or electrically by ropes or tethers. They are broadly classified based on the location of the power conversion mechanism: Ground-Gen (GG) and Fly-Gen (FG).

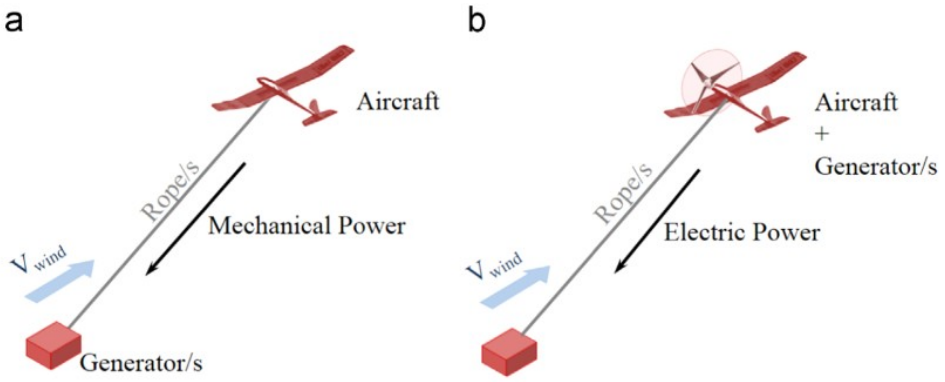


Figure 1.3: Example of Ground-Gen (a) and Fly-Gen (b) AWESs [5].

In Ground-Gen systems, the conversion of mechanical energy into electrical energy takes place on the ground. The tether transmits the mechanical power (traction force) generated by the airborne device to a winch-generator unit on the ground station.

These systems typically operate using a two-phase discontinuous cycle, known as the *pumping cycle*:

- Generation Phase (Reel-Out/Traction): the aircraft is driven in a high-power, cross-wind motion (circular or figure-eight paths) to maximize lift force and tether tension. The unwinding of the tether causes the generator to produce electricity;
- Recovery Phase (Reel-In/Retraction): the aircraft is controlled to minimize aerodynamic resistance (e.g., through side-slip or flagging maneuvers), reducing the energy consumed as the tether is reeled back in.

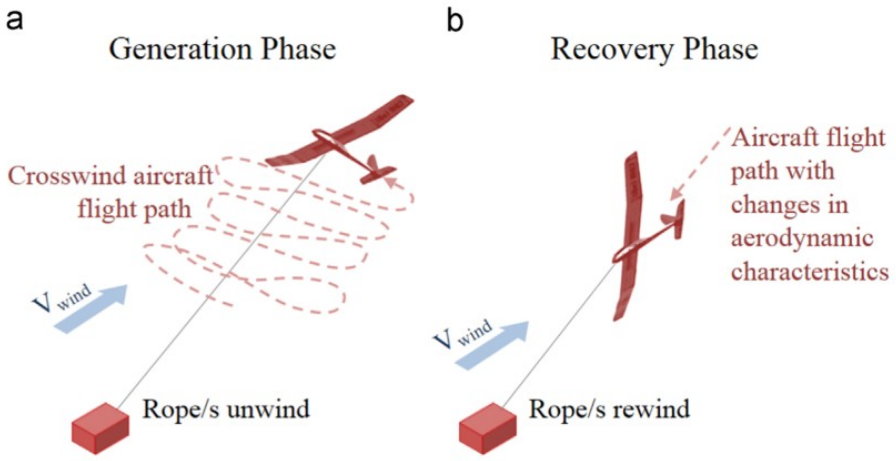


Figure 1.4: Scheme of the pumping cycle, showing Generation phase (a) and Recovery phase (b) [5].

The system achieves a net positive energy balance because the energy produced during the generation phase exceed the one consumed during the recovery phase. A notable drawback is the highly discontinuous power output, requiring electrical rectification as batteries or large capacitors.

Those systems are further distinguished by their ground architecture. In the fixed ground station configuration, also known as pumping kite qenerators (e.g., KiteGen Research, SkySails Power), the winch and generator remain stationary on the ground. Conversely, the moving ground station configuration relies on rail circuits or vertical axis generators (e.g., NTS Energie and other KiteGen Research concepts) to convert the motion induced by tether tension into a continuous or quasi-continuous power output [5].

In Fly-Gen systems, the conversion of wind energy into electrical energy takes place directly onboard the airborne platform, rather than at the ground station [5, 22]. The aircraft is equipped with one or more small scale turbine generator units, typically mounted along the wings or fuselage. The generated electricity is then transmitted to the ground through a conductive tether containing copper or aluminum power cables and fiber optic

lines for data transmission [31]. This configuration eliminates the need for a mechanical reel generator system on the ground, reducing moving parts and improving the continuity of power output.

Those systems generally operate in a steady state generation phase, during which the aircraft maintains a constant tether length while flying crosswind patterns at its operational altitude. The tether is only pulled out during takeoff or altitude adjustments and re-wound for landing procedures. The absence of a cyclic pumping operation allows those systems to deliver continuous electrical power [12, 13].

Most Fly-Gen architectures employ rigid airframes resembling gliders or drones, designed with high aerodynamic efficiency and equipped with embedded propellers that function as airborne wind turbines. Notable examples include the systems developed by Makani Power and Joby Energy, which pioneered the use of distributed electric generation onboard multi rotor airborne platforms [5, 31].

Although these prototypes successfully demonstrated autonomous flight and onboard power conversion, their large scale deployment remains limited due to technical challenges such as high mechanical loads on the tether, energy transmission losses and the complexity of autonomous control in variable atmospheric conditions.

### 1.2.2 Flight path

The classification of flight trajectories in AWES is a fundamental aspect of their aerodynamic and energetic design. Flight paths are defined by how aerodynamic forces are converted into useful mechanical or electrical power, identifying two main operational motion mode: crosswind flight and non-crosswind. Additional classifications also include rotational trajectories and hybrid or bimodal operational modes observed in some advanced systems [22].

Crosswind flight represents the most common and efficient operational flow and is considered the key to large scale energy generation. In this mode, the wing moves perpendicular to the ambient wind direction, exploiting an apparent wind speed much greater than the true one. This effect increase the aerodynamic forces, by a factor approximately equal to the system's lift-to-drag ratio, generating one to two orders of magnitude more power than non-crosswind configurations [5].

Specific trajectory patterns commonly used in crosswind operation include figure-eight paths and circular paths. In Ground-Gen systems, figure-eight trajectories are typically employed during the generation (reel-out) phase of the pumping cycle, where the wing

follows fast reciprocal crosswind maneuvers to maximize tether tension and energy yield. The circular flight path is commonly adopted in Fly-Gen systems, with the aircraft maintaining a constant tether length to ensure steady aerodynamic loading on the onboard turbines and achieve continuous power generation [31].

Non-crosswind or tether-aligned flight, refers to trajectories in which the wing's motion does not rely primarily on crosswind dynamics. Although these configurations simplify control and reduce tether drag, they generate lower power and result less efficient. Three main subcategories can be identified [5, 31]:

- Static flight: implemented in lighter-than-air systems such as aerostats or balloons that remain aloft due to buoyancy. These devices can access high altitude wind resources but the lack of crosswind acceleration mechanism lead to a limited power density;
- Tether-aligned flight: the wing's path aligns with the tether direction, minimizing aerodynamic resistance but reducing the swept area and overall energy extraction potential;
- Stationary trim condition: in some rigid-wing models, a steady aerodynamic equilibrium (trim) is maintained under uniform wind conditions, balancing lift, drag, and tether forces without active flight dynamics.

A further category includes rotational and operational trajectories, which describe specific flight configurations or stages of operation. Rotational systems employ multiple kite or wing elements moving along a circular path around a central axis, functioning similarly to a rotor. Some advanced Fly-Gen systems, such as the Makani prototypes, adopt a bimodal flight mode: vertical takeoff and landing (VTOL) using propellers for lift, followed by tethered circular flight for power generation [5, 22].

Typical maneuvers used in some operational stages are side-slip or flagging, to reduce lift allowing the wing to descend with minimal energy loss [31] and low-tension trajectory to minimize drag and power consumption during tether retraction in recovery phase on Ground-Gen systems.

### 1.2.3 Wing structure

An equally important aspect in terms of aerodynamic performance is the characterization of the wing. In the current landscape of AWE development, two main structural concepts have emerged: soft-wings, typically realized as fabric-based kites, and rigid-wings, designed as lightweight aircraft like gliders. The choice between these two configurations

involves a fundamental trade-off among cost, efficiency, durability and controllability.

Soft-wings are usually made of flexible materials such as ripstop nylon or laminated polyester, often with inflatable or ram-air cells that maintain shape through internal pressure. They are lightweight, inexpensive, easy to transport and replace, making them particularly suitable for small scale or prototype AWE systems. However, their aerodynamic efficiency is limited by shape deformation under load and their operational lifetime rarely exceeds a few hundred hours due to material fatigue and UV exposure. Moreover, precise autonomous control of soft-wings remains a major challenge, since their dynamic shape variation complicates flight modeling and control algorithms [5].

Rigid-wings, on the other hand, are built using composite structures, typically carbon fiber or fiberglass reinforced polymers, which ensure high stiffness and superior aerodynamic performance. These systems can operate at higher lift-to-drag ratios, resulting in greater energy conversion efficiency and more stable crosswind flight. Their structural integrity enables decades long lifetimes with proper maintenance, making them well suited for multi megawatt AWE prototypes and commercial systems. The main drawbacks of rigid-wings are their higher manufacturing cost, increased mass and the need for more complex takeoff and landing mechanisms.

In recent years, a clear trend has emerged within the AWE industry toward the adoption of rigid or semi-rigid-wings for large scale, power generating systems [3, 31]. This evolution reflects a growing emphasis on aerodynamic efficiency, flight stability and long-term reliability, all essential for achieving higher energy yields and reducing the overall Levelized Cost of Energy. Nevertheless, soft-wing systems continue to play a crucial role in research and early stage testing due to their lower cost, safety and ease of deployment. It is likely that both configurations will coexist in the near future, each serving different applications within the broader AWE ecosystem, ranging from portable small scale units to utility-grade offshore installations.

## 1.3 State of art

Airborne Wind Energy systems are still a relatively new technology, with most projects currently at the prototype or pilot stage and no fully operational farms yet in place. Despite this early stage, AWE has shown great potential to unlock high altitude wind resources and expand the role of wind power in the renewable energy mix. Over the past years, research in this field has grown rapidly, covering areas such as flight control, aerodynamic modelling, materials and energy conversion. This growing scientific interest

highlights both the challenges and the opportunities of AWE.

According to Trevisi et al. [27], a refined aerodynamic formulation including vortex wake effects allows for a more accurate description of power generation in crosswind AWE systems. The results show that fly-generation configurations often achieve higher performance than ground-generation systems, contributing to a deeper understanding of the aerodynamic behaviour of tethered kites and improving the predictive capability of power models used in system optimisation.

From a techno-economic perspective, Joshi et al. [12] developed a multidisciplinary design, analysis and optimisation framework to evaluate and scale ground-generation AWE systems. Through the integration of aerodynamic, structural and cost components, their integrated model identifies the parameters that most impact the LCoE. The study demonstrated that kite mass, tether lifetime and energy storage requirements are the dominant cost drivers, and that the economic optimum for current technologies lies between 100 kW and 1 MW. These findings are crucial in defining realistic development targets, showing how the cost structure of AWE differs substantially from that of conventional wind turbines, with operational costs representing a larger share of total expenditures.

In the field of structural design, Candade [4] presented the study Aero-structural Design and Optimisation of Tethered Composite Wings, which focuses on the design and optimisation of kites made of advanced composite materials. By coupling aerodynamic simulations with finite-element structural analysis, the research developed an optimisation framework aimed at reducing mass while maintaining aeroelastic stability and fatigue resistance. The results showed that optimised composite lay-ups and local reinforcements in critical areas, such as the tether attachment points, can reduce structural mass by up to 20% without compromising performance. This work provides one of the most comprehensive frameworks for the aero-structural design of kite based AWE systems, offering valuable insights into the development of lightweight, efficient and durable airborne structures suitable for large scale deployment.

Moving toward offshore applications, Trombini, Pasta and Fagiano [28] investigated the dynamic interaction between a pumping AWE system and a floating spar-buoy platform. Their model combines a six degree of freedom representation of the floating structure with a detailed dynamic model of the kite and tether, allowing the evaluation of the mutual influence between aerodynamic loads and hydrodynamic motion. The results indicate that the oscillations of the platform have a limited effect on flight stability; however, the tether-force fluctuations may resonate with the natural frequencies of the platform, leading to increased fatigue stresses. To mitigate this phenomenon, the authors proposed

a control strategy that modifies the kite's flight trajectory to avoid resonant conditions, representing an important step towards the safe and reliable implementation of offshore AWE systems.

Beyond the technological aspects, Schmidt et al. [23] conducted the first systematic review addressing the social acceptance of AWE. By analysing forty publications, the authors identified five main factors that could influence public perception: safety, visibility, acoustic emissions, ecological impact and siting. The review revealed that, despite optimistic assumptions, empirical evidence remains scarce and that most studies are still based on theoretical considerations rather than field data. The authors stress the importance of involving social sciences in the future development of AWE to better understand public attitudes, anticipate concerns and promote transparent regulatory and communication strategies.

Taken together, these studies reveal a research field that is expanding rapidly but still fragmented across disciplines. Aerodynamic and structural modelling are becoming more accurate, cost analyses are clarifying the economic feasibility of different configurations and early offshore and social investigations are broadening the understanding of the environmental and societal implications of this technology. Overall, the literature converges on the idea that Airborne Wind Energy has the potential to complement traditional wind power production. Nevertheless, achieving this potential will require further progress in automation, material optimisation, large scale experimental validation and integration into the broader renewable energy landscape.

## 1.4 Outline

The limited number of studies concerning Airborne Wind Energy within the Italian context raises an essential question: whether this emerging technology could realistically find a place in Italy's future renewable energy landscape. This work addresses this question by examining the potential applicability of Airborne Wind Energy systems in offshore environments, which represent one of the most promising deployment scenarios for the country.

The first objective of the work is to understand whether Italian offshore winds can provide sufficient and stable resources to support the operation of an AWE system. To address this question, an extensive analysis of the available atmospheric reanalysis datasets was carried out. These datasets were compared in terms of spatial resolution, representation of high altitude winds and suitability for describing the operating conditions typical of airborne technologies. The comparison made it possible to identify the dataset most appropriate

for this research, forming the basis for a reliable characterisation of the offshore wind resource.

Once the wind environment was defined, the thesis moved to assess the technological feasibility of offshore AWE deployment. This was achieved through the development of a numerical model capable of estimating the Annual Energy Production (AEP) of a representative airborne unit. The model combines the selected wind dataset with the real power curve of the considered AWE system, allowing the computation of the expected producible energy under realistic offshore conditions in the Italian seas. This step provides the first quantitative indication of whether airborne systems could operate effectively within the local wind regime.

Building upon the evaluation of producibility, the study then addresses the economic dimension of offshore AWE. A preliminary techno-economic assessment was performed through the estimation of the Levelised Cost of Energy, which expresses the average cost of electricity generation over the system lifetime. Since no detailed cost data for offshore airborne systems currently exist, an existing cost model from the literature was analysed and adapted to reflect the specific characteristics of AWE technology and the offshore context examined in this work. This adaptation enabled the construction of an initial cost framework for an offshore airborne wind farm and allowed a first estimate of its economic viability.

Overall, the thesis combines wind resource assessment, technological evaluation and an early stage economic analysis to provide the first region-specific investigation of the potential of Airborne Wind Energy in Italian offshore areas. The results aim to offer new knowledge that is currently absent in the literature and to support future research directions, policy considerations and the preliminary evaluation of investment opportunities.

# 2 | Technical Analysis

## 2.1 Scope definition

The Italian offshore domain considered for this study includes the Adriatic Sea, the Tyrrhenian Sea, the Ionian Sea and the Sicilian Channel, excluding nearshore areas where installation of AWE systems would be restricted by different kind of constraints.

The data collection phase represented one of the most challenging stages of this analysis. Several datasets required for the offshore assessment were not always complete, up to date or immediately compatible with MATLAB-based processing. Particular effort was devoted to gathering, validating and harmonizing multiple geospatial layers to ensure a consistent and reliable input database for subsequent AEP computations and mapping activities in ArcGIS.

All spatial datasets were obtained from the online repository of the European Marine Observation and Data Network (EMODnet), a public platform that provides standardized marine and coastal data for European waters. The downloaded data, primarily in shapefile format, were selected from different EMODnet thematic portals, focusing on human activities, environmental protection and marine traffic.

The datasets were categorized according to their geometric representation:

- Polygonal layers:
  - *E*xclusive Economic Zones (EEZ);
  - *Protected Areas under CDDA* (Common Database on Designated Areas);
  - *Active Licenses for Oil and Gas Exploitation*;
  - *Natura 2000 Protected Areas* (Habitats and Birds Directives sites);
  - *Nationally Designated Areas.*
- Point-based layers:
  - *Main Ports and Harbors*;

  - *Offshore Wind Farms*;
  - *Protected Sites* with specific geographic coordinates.

– Linear layers:

  - *Maritime Routes and Traffic Density Indexes*, describing major navigation corridors and their respective usage intensity.

The Exclusive Economic Zones (EEZ), delineating Italy's maritime jurisdiction were first acquired and processed. They represents a maritime area extending from the baseline of the coastal State out to a defined limit, typically up to 200 nautical miles, within which the State holds sovereign rights to explore and exploit marine resources, including wind and seabed resources.

For the purpose of this study, the Italian EEZ polygons provide the spatial boundary within which the wind resource analysis and Annual Energy Production computations are performed. By applying the EEZ boundary, the analysis ensures that only legally available marine areas for national development are considered, thus aligning the assessment with both maritime law and strategic deployment constraints.


Figure 2.1: Italian maritime Exclusive Economic Zones (EEZ).

Following the identification of the Italian EEZ boundaries, the main marine spatial constraints were preliminarily overlaid on the defined domain, to refine the areas available for AWE deployment. These constraints, previously listed, include environmentally protected areas, active oil and gas concessions, existing offshore infrastructures and maritime traffic routes. The spatial overlay allowed for a first exclusion of zones where the installation of AWE systems would be legally or technically infeasible. Figure 2.2 illustrates the distribution of these marine restrictions within the Italian offshore domain.

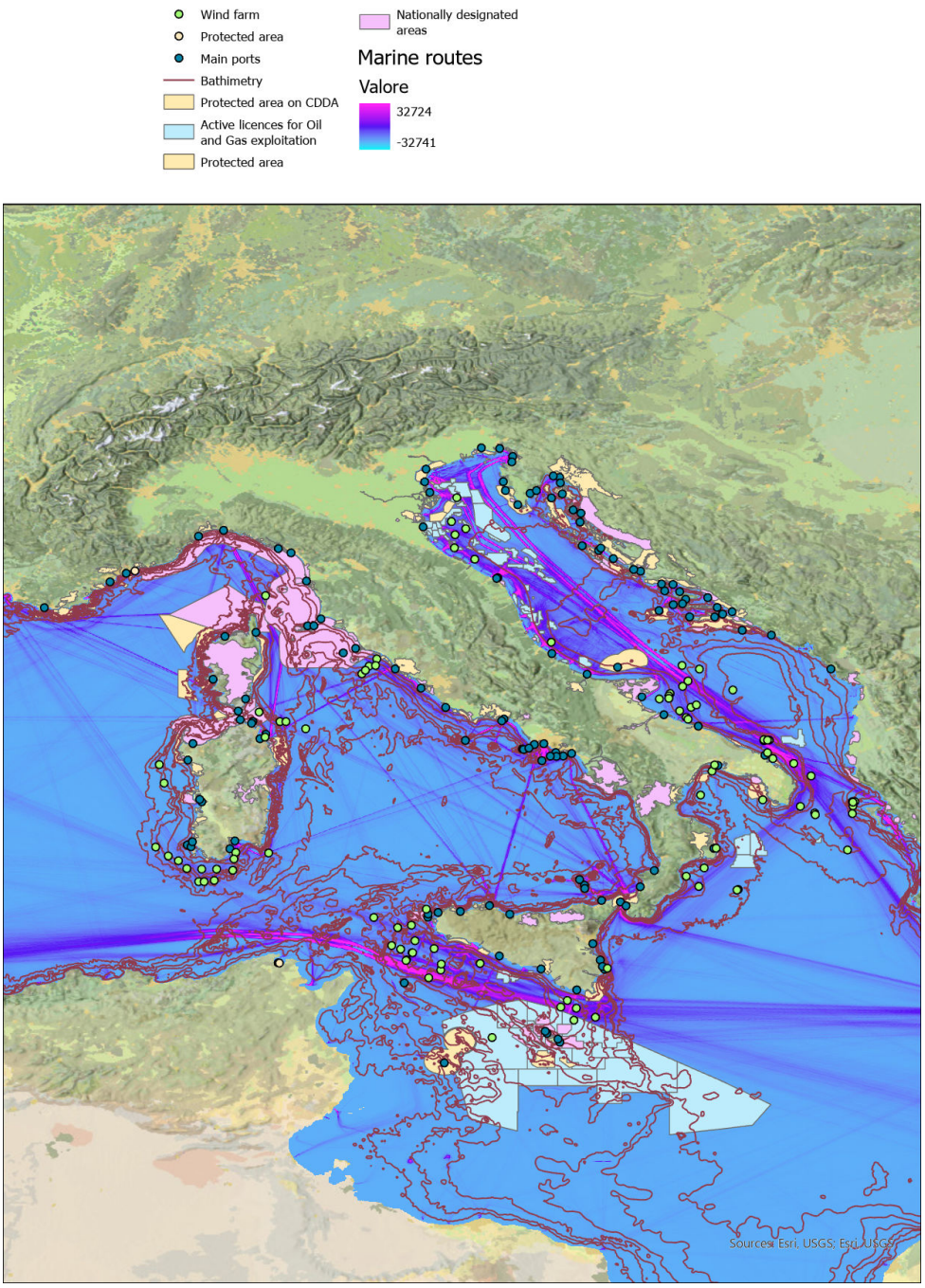


Figure 2.2: Italian offshore area constraints.

Due to the extensive quantity of geospatial data and the large computational domain, the analysis could not be carried out an itemized resolution for the entire Italian offshore area. Instead, the study adopted a discrete grid-based approach, dividing the maritime domain into smaller cells (as detailed in Section 2.5). This approach allowed for a manageable computation of AEP while preserving an acceptable level of spatial accuracy. Linear and point constraints, such as individual ports, shipping routes and offshore wind farm

locations, were not incorporated directly into the AEP computation, as they could not be spatially resolved within the selected grid size.
Polygonal constraints, including environmental and regulatory zones (e.g., Natura 2000, CDDA, and nationally designated areas), were considered and overlaid into the grid to identify exclusion zones and to delineate suitable areas for potential AWE deployment.

## 2.2 Reference AWE system

The selected Airborne Wind Energy system for this analysis was the *SkySails Power Venyo (PN–14)* model, a ground-generation system equipped with a soft-wing (ram-air kite) and a mobile ground station [24].

Figure 2.3: SkySails Venyo (PN–14) system render[24].

The technical specifications of this system report a rated power up to 200 kW and an operational altitude of approximately 200 m, with an average Annual Energy Production of 760 MWh at a mean wind speed of 9 m/s. The power curve was obtained from the manufacturer's technical datasheet and subsequently digitalized for computational use (Figure 2.4).

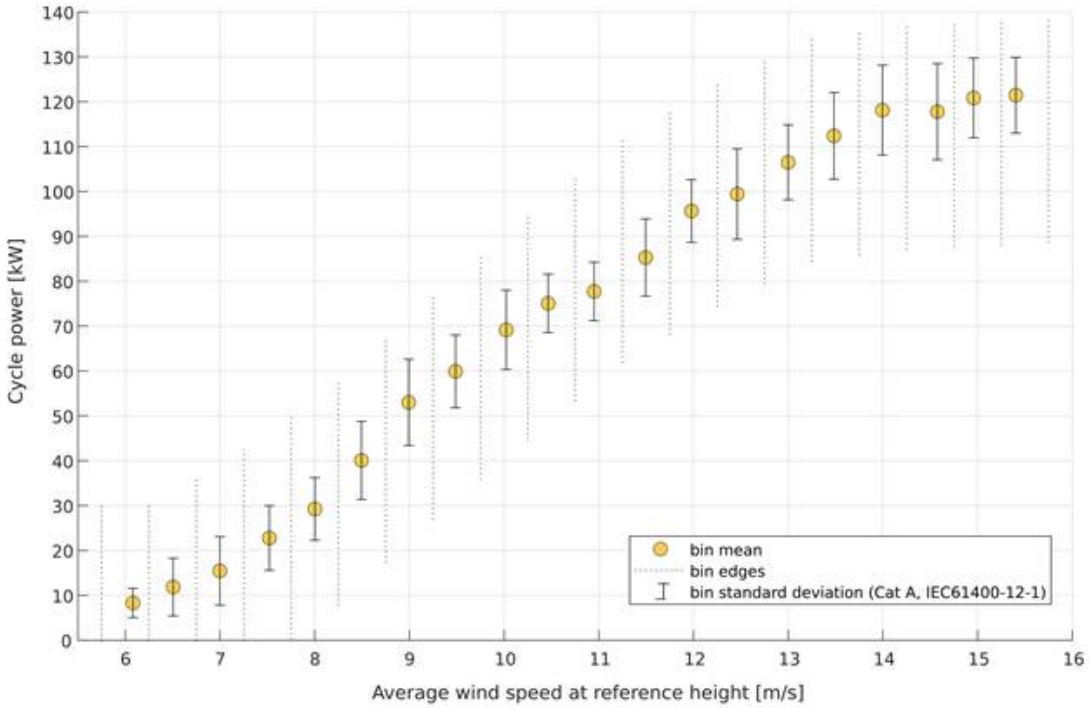


Figure 2.4: Power curve of the SkySails Venyo (PN–14) system.

Even if is an empirical curve, represents the best available estimation of system performance. It is not supported by any dedicated certification framework, since no formal criteria for validating AWE performance metrics have yet been established. For this reason, the curve should be considered indicative rather than certified, reflecting the early stage of standardisation in Airborne Wind Energy.

A second assumption concerns the operational hours of the system. Current AWE prototypes are not autonomous and require continuous operator supervision, which limits their realistic availability and prevents uninterrupted operation. Nevertheless, the assessment assumes 8760 annual operating hours, without accounting for downtime related to supervision, maintenance or repair. This simplification was introduced to isolate the influence of the wind resource and system parameters on AEP and LCoE, acknowledging that real availability would be lower under present technological conditions.

A further simplification relates to the treatment of the operating height. Although AWE systems move along crosswind trajectories with significant vertical excursions, the modelling carried out in this thesis relies on a fixed reference altitude to derive wind statistics and AEP. This approximation allows a consistent comparison between datasets and scenarios but does not capture the full variability associated with dynamic flight paths. Future work supported by more detailed aerodynamic and flight control models will be

needed to lift this limitation.

## 2.3 Dataset

The development of atmospheric reanalysis is one of the most important step foreword in modern climate and meteorological modelling. Since the 1980s, all the progresses in the numerical weather prediction and the growing availability of global observations, have made possible to reconstruct past atmospheric conditions in a consistent and coherent way [8].

A reanalysis combines a wide range of observations taken from surface stations, radiosondes, buoys and satellites, producing datasets that describe the state of the atmosphere, land surface and ocean over a multi-year period in a homogeneous way [7].

The main idea behind reanalysis is to get around the gaps and inconsistencies that appear in regular weather analyses when forecasting models are updated. Reanalysis aims to create a continuous and uniform picture of the climate system over time, using a single and consistent model setup for the entire period.

The role of reanalysis in climate monitoring is now widely recognised. Climate reanalyses provide a comprehensive representation of the atmosphere, land and ocean through time, combining heterogeneous observations with advanced numerical models to produce continuous meteorological and climate fields in both time and space. For this reason, reanalysis data has become an irreplaceable resource for climate and meteorological research, supporting the study of long-term trends, climate extremes and the natural variability of the Earth system [8].

The European Centre for Medium-Range Weather Forecasts (ECMWF) has played a leading role in developing successive generations of reanalysis. With increasing computational power and an expanding archive of satellite data, reanalysis have reached higher spatial and temporal resolutions, culminating in ERA5, the fifth generation global reanalysis produced under the Copernicus Climate Change Service [11]. Reanalysis products now are the basis of atmospheric and climate research, offering a continuous, physically consistent depiction of the coupled Earth system. They are fundamental for studying climate variability and long-term trends, validating numerical models, and supporting a wide range of operational and scientific applications, from seasonal forecasting to energy system analysis.

One of the most relevant fields of application is wind energy resource assessment. Reanalysis datasets such as ERA5 provide hourly information on wind speed and direction,

atmospheric stability and turbulence, key parameters for evaluating wind energy potential both onshore and offshore. They enable the estimation of wind resources in regions with limited observation and long-term analysis of wind variability, which is critical for energy system planning.

Reanalysis like ERA5 exhibits strong spatial and temporal consistency and are particularly reliable over marine environments, where the absence of complex orography reduces modelling uncertainties. However, their relatively rough horizontal resolution (31 km) limits the ability to capture small scale processes, such as wind shear, that can affect energy production estimation.

In coastal or mountainous regions, more detailed representation often requires the use of regional reanalysis such as CERRA, which provides a more accurate representation of weather conditions [17].

Reanalysis datasets also play a strategic role in the energy transition context, helping to identify and quantify wind energy droughts, as extended periods of low wind speed that constrain power generation. Detecting such events is essential for planning resilient and low carbon energy systems.

Because they provide a continuous, vertically resolved description of the wind field, reanalyses constitute a key resource for designing and optimizing modern AWE systems, for estimating the capacity factor and Levelized Cost of Energy of both onshore and offshore projects.

In summary, atmospheric reanalysis have become indispensable datasets for both scientific and engineering applications. In the field of wind energy, their combination of global consistency, temporal continuity and accessibility make them essential tools for assessing wind resources, forecasting production variability and supporting the design of sustainable and integrated energy systems.

### 2.3.1 ERA 5

ERA5 is the fifth generation global atmospheric reanalysis produced by the European Centre for Medium-Range Weather Forecasts (ECMWF) as part of the Copernicus Climate Change Service (C3S). It provides a continuous reconstruction of the atmosphere, ocean waves and land-surface variables from 1940 to the present, with hourly data at about 31 km spatial resolution and 137 vertical levels up to 0.01 hPa.

Compared to the previous ERA-Interim reanalysis, ERA5 offers major improvements in data assimilation, spatial resolution and the number of observations included, especially

satellite data. The goal is to provide a consistent and detailed description of the global climate, suitable for both weather and climate studies.

ERA5 is based on ECMWF's Integrated Forecasting System (IFS) [11], cycle 41r2, which couples the atmosphere, land surface and waves. It uses a four dimensional variational assimilation (4D-Var) system with a 12-hour window, integrating millions of observations from surface stations, aircraft, radiosonde, buoys and satellites.

A key innovation is the ten-member Ensemble of Data Assimilations (EDA), which estimates the uncertainty of the analysis by slightly perturbing the input data and model physics. This allows users to quantify confidence in the reanalysis, especially in data-sparse regions like the oceans.

ERA5 also includes an improved treatment of clouds, radiation and surface processes through the HTESSEL land model and the ECWAM wave model, providing a better representation of surface roughness and air–sea interactions, important aspects for offshore wind applications.

It offers a wide set of atmospheric and surface variables such as temperature, pressure, humidity and wind components. For wind studies, the most relevant fields are $u$ and $v$ wind speed components at 10 m and 100 m, which is close to the hub height of modern turbines.

Thanks to its hourly resolution and global coverage, ERA5 can capture short term wind variations, like diurnal cycles and seasonal patterns, as well as long-term trends. It is also widely used to study vertical wind profiles, including wind shear and veer, which affect energy yield and turbine design.

ERA5 has shown a clear performance improvement compared to older reanalyses.
It provides better agreement with observations in terms of temperature, precipitation and especially wind speed. Several studies have confirmed its reliability for renewable energy assessments, both onshore and offshore.

However it can still underestimate wind speeds at turbine height and overestimate low-wind periods, especially under stable atmospheric conditions. Despite these limits, it remains the most widely used dataset for wind resource analysis, grid integration studies and LCoE estimation, thanks to its global consistency and open availability.

In summary, ERA5 represents the current standard in global reanalysis: it combines advanced assimilation methods, extensive observational data and a high spatial–temporal resolution, making it a fundamental tool for both climate research and wind energy studies [11].

### 2.3.2 CERRA

The Copernicus European Regional Reanalysis (CERRA) is the most recent high-resolution regional reanalysis developed within the Copernicus Climate Change Service (C3S).
It provides a detailed and physically consistent reconstruction of the European climate from 1984 to the present, with a horizontal resolution of 5.5 km, much finer than the 31 km of ERA5.

CERRA was designed to complement global reanalyses like ERA5 by providing a more accurate representation of local weather and climate processes, especially in regions with complex topography, strong land–sea contrasts and highly variable wind conditions.
Its main goal is to capture mesoscale atmospheric phenomena, such as local winds, sea breezes, mountain effects and precipitation patterns, that are often smoothed out in coarser global datasets.

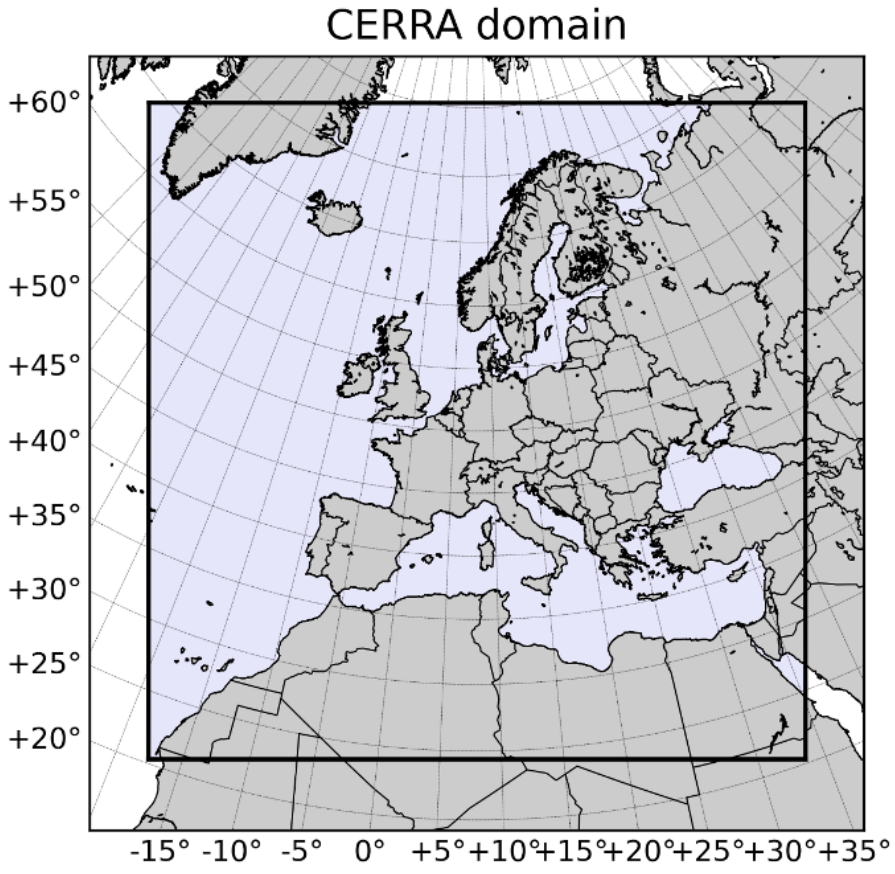


Figure 2.5: CERRA domain [6].

CERRA is based on the HARMONIE-AROME numerical weather prediction model, part of the ALADIN–HIRLAM modelling system [17] used operationally by several European

meteorological services. It employs a three dimensional variational data assimilation (3D-Var) scheme, similar in structure to ECMWF's system but adapted to a smaller regional domain.

This system is driven by boundary conditions from the global ERA5 reanalysis, ensuring large scale consistency between the two datasets. It assimilates a wide range of observations, including both conventional data, from surface stations, aircraft and radiosondes and non conventional observations such as radar measurements, satellite radiances and high resolution data from national networks. This combination allows for a denser and more detailed observational coverage over Europe. The model is defined on 65 vertical levels up to 10 hPa and is coupled to a high resolution surface data assimilation system that accounts for snow, soil moisture and surface temperature variability.

One of CERRA's key features is its Ensemble of Data Assimilations (CERRA-EDA), which consists of six perturbed members. The ensemble provides an estimate of the background and observation uncertainties and allows users to assess confidence levels in the reanalysis, similarly to the EDA system in ERA5 but optimized for regional scales.

Additionally, CERRA is complemented by CERRA-Land, a land-surface reanalysis that further downscales the surface parameters to 2.5 km resolution, improving the representation of soil moisture, snow cover and surface fluxes.

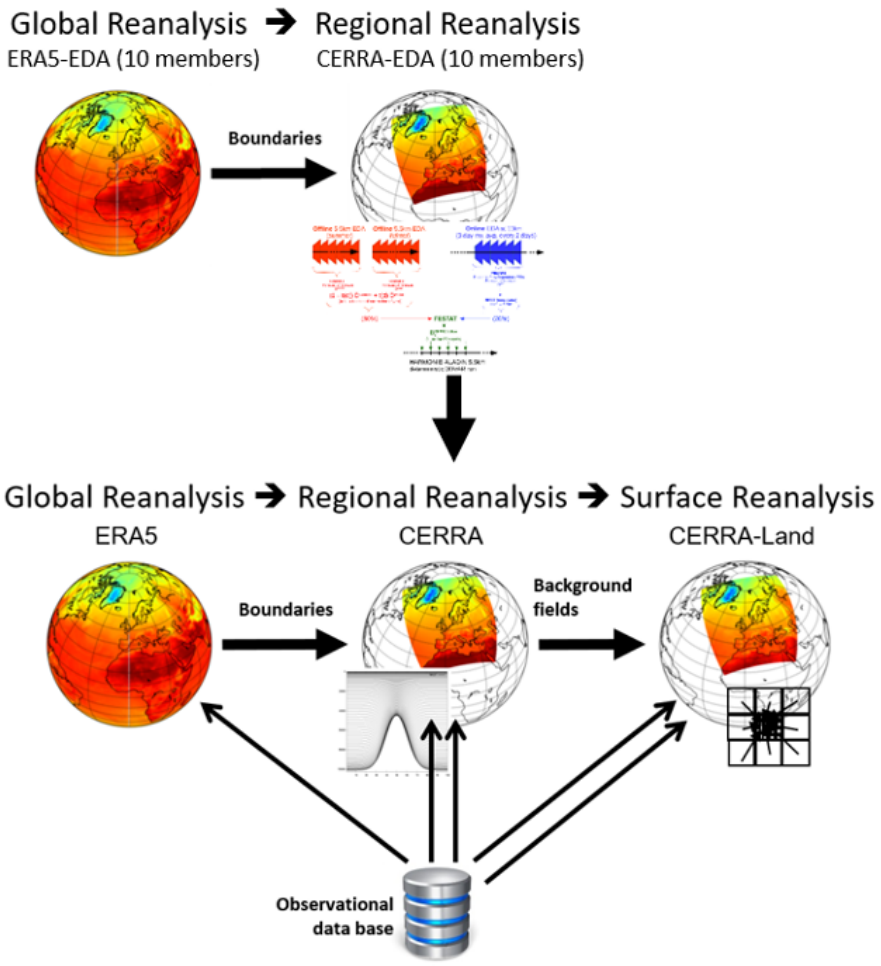


Figure 2.6: CERRA production chain [6].

The CERRA dataset provides hourly outputs for a wide range of meteorological variables, including temperature, pressure, humidity, precipitation and wind velocity at 10 m and higher levels. Thanks to its finer resolution and the use of regional observations, CERRA captures local atmospheric features much better than ERA5. It reproduces complex orography, small islands and coastlines with higher accuracy, leading to more realistic local wind and precipitation patterns.

A study conducted over the Alpine region showed that CERRA provides a significant improvement in the representation of near-surface temperature, wind, and precipitation fields, particularly in mountainous areas and coastal zones affected by sea-breeze circulations [17].

CERRA's high spatial resolution makes it particularly suitable for wind resource assessment and regional energy modelling. While ERA5 provides a consistent global reference, its 31 km grid often smooths out orographic effects and local wind regimes. In con-

trast, CERRA can resolve small scale circulations and topographically driven winds that strongly influence local energy potential, especially in coastal and mountainous areas.

For example, recent studies highlight that regional reanalyses like CERRA tend to reproduce stronger and more variable winds, with reduced bias compared to ERA5 when validated against local Mast and LiDAR data. This makes them particularly valuable for high resolution mapping of AEP and for improving LCoE estimations in both onshore and offshore wind projects within Europe [17].

CERRA extends the capabilities of global reanalyses to the regional scale. Its higher resolution and denser observation network enable a much better description of local atmospheric processes, leading to improved accuracy in temperature, precipitation and wind fields. Although its coverage is limited to the European domain, CERRA represents a valuable dataset for climate and renewable energy studies, particularly where local wind dynamics play a key role.

## 2.4 Dataset comparison

In this section, the methodology used to compare wind speed data at different heights is presented. The goal is to assess the consistency between the two over the course of one year and to evaluate how any discrepancies may affect the calculation of the Annual Energy Production. The entire analysis was carried out in MATLAB, combining NetCDF data extraction, temporal aggregation, statistical comparison and energy modeling based on the power curve.

### 2.4.1 Data acquisition

The analysis was carried out using reanalysis data for the year 2022.

ERA5 provides hourly wind components ($u$ and $v$) with a spatial resolution of 0.25°, while CERRA provides wind speed data every three hours, with a spatial resolution of approximately 5.5 km.

The analysis was performed on observation points corresponding exactly to an ERA5 grid node, where the model provides a defined wind speed value. Around this position, a reference ERA5 cell was defined, representing the spatial resolution and area of influence of the model. Within this cell, all CERRA grid points were identified, and their spatial average was computed to obtain an equivalent CERRA value.

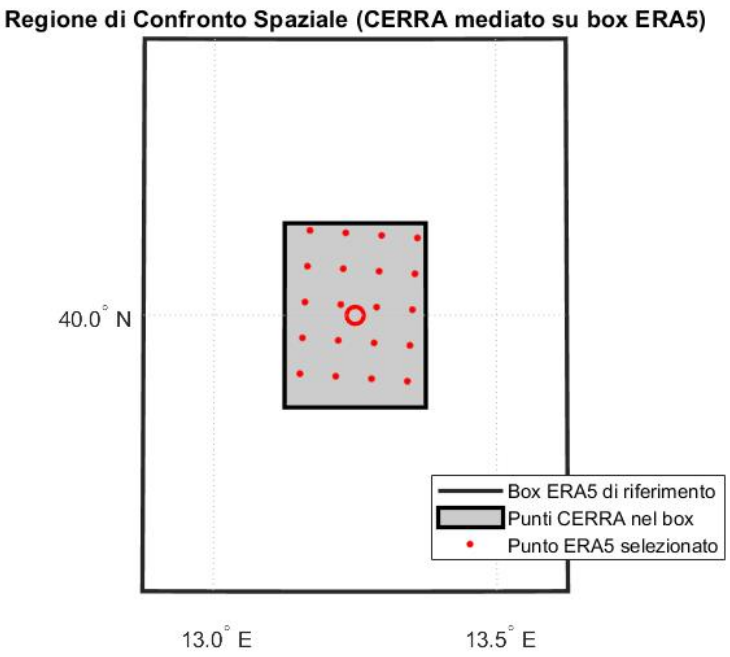


Figure 2.7: Representation of area considered in the analysis.

This approach ensures a consistent scale comparison between the ERA5 data and the spatially averaged CERRA data.

### 2.4.2 Pre-processing and temporal aggregation

CERRA directly provides the wind speed magnitude, while for ERA5 the horizontal wind components were combined to obtain the wind speed:

$$v = \sqrt{u^2 + w2} \tag{2.1}$$

where $u$ is the east-west wind component and $w$ is the north-south wind component.

Since the temporal resolutions differ, both datasets were aggregated into daily and monthly averages. Daily means were computed over blocks of 24 values for ERA5 and 8 values for CERRA, while monthly averages followed the standard calendar basis. This procedure allowed a direct comparison of seasonal and annual trends.

The ERA5 model provides wind components up to a maximum height of 100 m, whereas CERRA includes data up to 500 m altitude. To compare the two datasets at heights above 100 m, ERA5 wind speeds were extrapolated from a known height $z_1$ to a target height $z_2$ using the commonly adopted *power law*, expressed as:

$$v(z_2) = v(z_1)\left(\frac{z_2}{z_1}\right)^{\alpha} \tag{2.2}$$

where:

- $v(z_1)$ is the wind speed at the known height $z_1$;
- $v(z_2)$ is the estimated wind speed at the new height $z_2$;
- $\alpha$ is the power-law exponent, typically assumed equal to 0.14 for offshore conditions.

### 2.4.3 Statistical comparison

A statistical analysis was performed to assess the agreement between the two datasets. The following indicators were considered:

– Mean wind speed ($\bar{v}$): average value of the time series and provides a synthetic measure of the mean wind intensity

$$\bar{v} = \frac{1}{N}\sum_{i=1}^{N} v_i \tag{2.3}$$

where $v_i$ is the wind speed at time $i$ and $N$ is the total number of observations;

– Standard deviation ($\sigma$): measure of the dispersion of wind speed values around the mean, quantifying the temporal variability of the dataset

$$\sigma = \sqrt{\frac{1}{N-1}\sum_{i=1}^{N}(v_i - \bar{v})^2} \tag{2.4}$$

A higher value of $\sigma$ indicates greater wind variability over the analyzed period;

– Root Mean Square Error (RMSE): absolute difference between the two datasets in physical units (m/s)

$$\mathrm{RMSE} = \sqrt{\frac{1}{N}\sum_{i=1}^{N}(v_{\mathrm{ERA5},i} - v_{\mathrm{CERRA},i})^2} \tag{2.5}$$

Values of RMSE close to zero indicate a good agreement between the two time series;

– Pearson correlation coefficient (r): measure of the temporal coherence between the two datasets, regardless of their absolute values

$$r = \frac{\sum_{i=1}^{N}(v_{\text{ERA5},i} - \bar{v}_{\text{ERA5}})(v_{\text{CERRA},i} - \bar{v}_{\text{CERRA}})}{\sqrt{\sum_{i=1}^{N}(v_{\text{ERA5},i} - \bar{v}_{\text{ERA5}})^2 \sum_{i=1}^{N}(v_{\text{CERRA},i} - \bar{v}_{\text{CERRA}})^2}} \tag{2.6}$$

The coefficient $r$ ranges between -1 and +1.
Values close to +1 indicate strong positive correlation (similar temporal trends), while values near 0 suggest little or no relationship between the datasets.

### 2.4.4 AEP calculation and comparison

To estimate the Annual Energy Production associated with each wind speed series, the technology power curve was applied. The wind speed time series, for both the dataset, were divided into classes (bins) of 0.5 m/s width.

For each class, the number of occurrences $n_k$ and the corresponding relative frequency $f_k$ were computed as:

$$f_k = \frac{n_k}{N} \tag{2.7}$$

where $N$ is the total number of available data points in the series.

Since the observation period covers a full year, the relative frequency $f_k$ can be converted into equivalent annual hours:

$$H_k = f_k \times 8760 \tag{2.8}$$

where 8760 are the assumed operative hours in a year.
This value indicates how many hours, on average, the wind blows within the $k$-th speed interval.

For each wind speed class, the annual energy produced is obtained as the product between the turbine's average power in that class and the corresponding equivalent annual hours:

$$E_k = P_k \times H_k \tag{2.9}$$

where:

- $E_k$ is the annual energy produced in the $k$-th bin [kWh];
- $P_k$ is the average turbine power corresponding to the speed $v_k$ [kW];
- $H_k$ is the equivalent annual number of hours [h].

The total Annual Energy Production is obtained by summing the contribution of all wind speed classes:

$$AEP = \sum_{k=1}^{M} E_k = \sum_{k=1}^{M} P_k \times H_k \tag{2.10}$$

where $M$ is the total number of considered bins.
The result is expressed in kWh/year and then converted into MWh/year.

The analysis was performed at two reference heights of 100 m and 300 m. The 100 m level corresponds to the highest wind data directly available from ERA5, while 300 m was selected as a representative value within the typical operating range of AWE systems, which harness stronger and more stable winds at higher altitudes.

## 2.5 AEP assessment for the Italian offshore domain

To evaluate how Airborne Wind Energy could be integrated within the current energy market, particularly within the Italian offshore energy context, an estimation of the Annual Energy Production over Italian seas was carried out. The AEP represents the theoretical maximum amount of energy that could be harvested by the technology, assuming continuous operation under the wind conditions of the entire Italian maritime area.

### 2.5.1 Methodology and wind data processing

After defining the available maritime domain, a computational grid with a resolution of 10 km $\times$ 10 km was generated, covering all suitable offshore areas within the Italian seas. This discretization allow to evaluate the local wind energy potential keeping the computational effort manageable across large marine areas.

Within each grid cell, nine representative points were selected in a uniform way inside the grid.

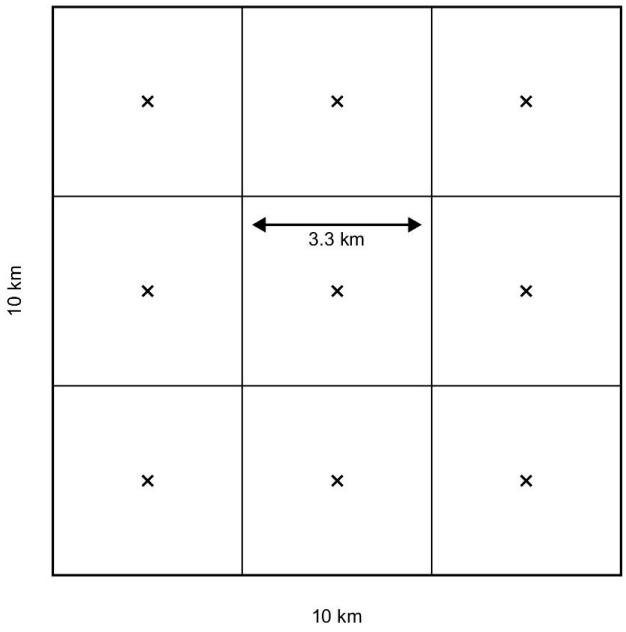


Figure 2.8: Representation of the grid cell into nine sub-cells.

For each of these points, wind speed data from reanalysis datasets were processed on MATLAB to derive a Weibull probability distribution, characterized by the shape parameters $k$ and the scale parameters $a$ , as defined in Equations 2.11 and 2.12.

$$f(v) = \frac{k}{a}\left(\frac{v}{a}\right)^{k-1} \exp\left[-\left(\frac{v}{a}\right)^{k}\right] \tag{2.11}$$

where:

- $v$ is the wind speed [m/s];
- $k$ is the shape parameter [-];
- $a$ is the scale parameter [m/s].

The parameters $k$ and $a$ were derived from statistical computation of the wind speed time series at each grid point using the relations:

$$k = \left(\frac{\sigma_v}{\overline{v}}\right)^{-1.086}, \quad a = \frac{\overline{v}}{\Gamma\left(1+\frac{1}{k}\right)} \tag{2.12}$$

where $\Gamma$ denotes the Gamma function.

The expected power output $\overline{P}$ for each cell was then computed as:

$$\overline{P} = \int_{v_{\text{cut-in}}}^{v_{\text{cut-out}}} P(v)\, f(v)\, dv \tag{2.13}$$

where $P(v)$ is the our reference power curve of the AWE system, and $v_{\text{cut-in}}$ and $v_{\text{cut-out}}$ selected are respectively 5 m/s and 16 m/s respectively.

Using the wind distributions and the power curve of the selected AWE system, the expected power output and the corresponding Annual Energy Production were computed for each point according to the relation:

$$\text{AEP} = 8760 \times \overline{P} \quad [\text{kWh/year}] \tag{2.14}$$

Consequently, nine AEP values were obtained for every 10 km × 10 km cell. The average AEP value of each cell $\overline{AEP}_{cell}$, was then calculated as:

$$\overline{AEP}_{cell} = \frac{1}{N} \sum_{i=1}^{N} AEP_i, \qquad N = 9 \tag{2.15}$$

This average represents the expected annual energy yield per installation within that specific portion of sea.

To obtain the total energy potential, $\overline{AEP}_{cell}$ was multiplied by the number of Airborne Wind Energy systems $n_{AWE}$ that can be installed within each cell, in accordance with the technological spacing constraints of the selected device, imposing a spacing of 500 m between each installed unit.

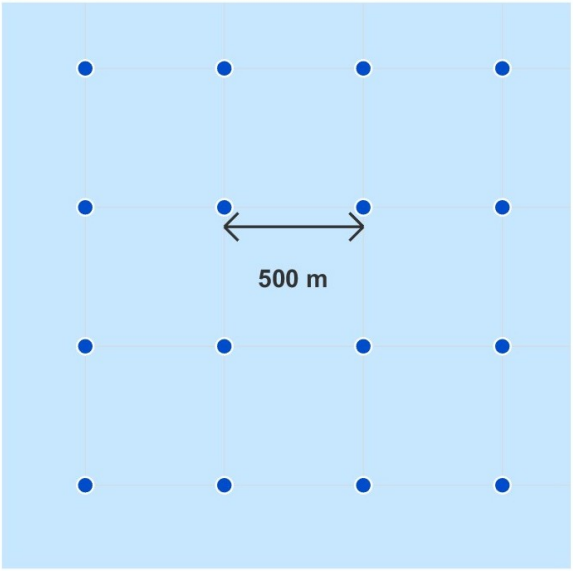


Figure 2.9: Representation of the AWE distribution.

The total AEP of the Italian offshore domain was then computed as the sum of all cell contributions:

$$AEP_{total} = \sum_{j=1}^{M} \overline{AEP}_{cell,j} \cdot n_{\mathrm{AWE},j} \tag{2.16}$$

where $M$ represents the total number of cells considered after applying spatial constraints and exclusion zones.

This procedure ensures that spatial variability in wind conditions is adequately represented, while maintaining computational feasibility. By aggregating cell-level results, the model provides an estimate of the total AEP achievable from AWE technology over the Italian offshore areas, considering both the available wind resource and the feasible technological deployment density.

The entire procedure described above was applied with both wind datasets ERA5 and CERRA in order to ensure a consistent comparison of their performance. Calculations were carried out at reference heights of 100 m and 300 m, corresponding respectively to the typical hub height of conventional offshore wind turbines and to the operational range of AWE systems. To account for inter-annual variability, the analysis was repeated for three consecutive years 2022, 2023 and 2024 providing a comprehensive temporal characterization of the wind resource and the resulting energy yield.

# 3 | Results of Technical Analysis

The purpose of this chapter is to present and discuss the results of the first stage of the analysis. Section 3.1 summarises the comparison between the two atmospheric datasets, highlighting their differences and implications for wind characterisation. Section 3.2 then builds on these findings to report the Annual Energy Production estimates derived from the modelling framework introduced in Sections 2.4 and 2.5.

## 3.1 Results of dataset comparison

Several geographical points within the study area were examined to assess the statistical consistency between the ERA5 and CERRA datasets. The following subsections present the results obtained at the two reference operating heights considered in this section.

### 3.1.1 Dataset comparison at 100 m

In the following figures, are reported the monthly evolution of the mean wind speed and the corresponding standard deviation, for the ERA5 and CERRA datasets at 100 m above ground level, in two caratteristic site. We can divede the results obtained in two main categories: the one in open sea and the one closer to the coast.

At the offshore site, as shown in Figure 3.1, the differences between ERA5 and CERRA are minimal. The monthly mean wind speeds almost coincide throughout the year and the variability represented by the standard deviation is comparable for both datasets, with largely overlapping error bars. The correlation factor between the two time series is around 0.98, indicating a strong temporal coherence and a consistent seasonal pattern when surface and topographic conditions are homogeneous. The table 3.1 summarizes the main wind speed statistics for ERA5 and CERRA.

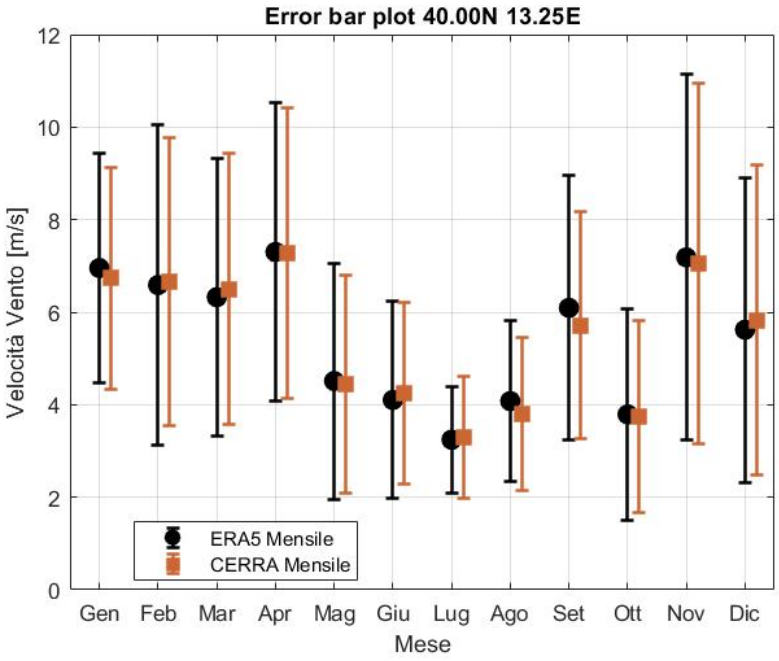


Figure 3.1: Error bar plot at 100m in offshore location.

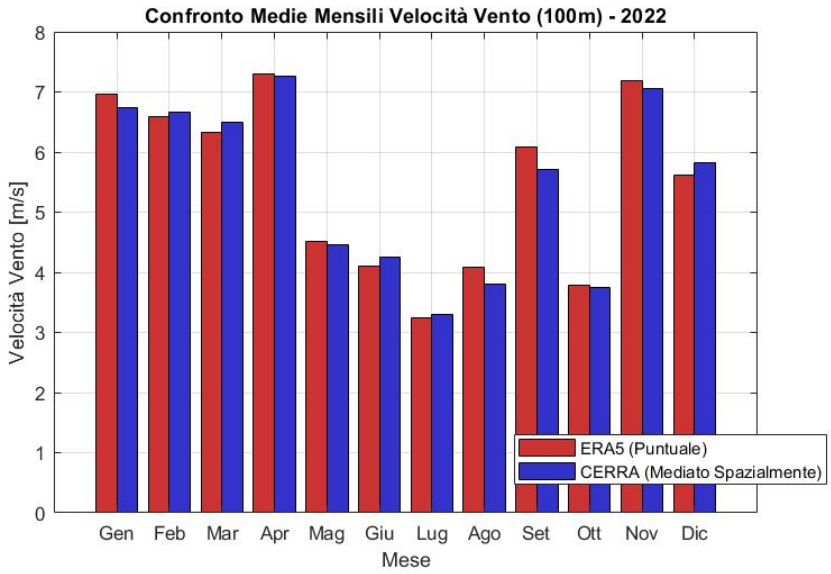


Figure 3.2: Average wind speed at 100 m for ERA5 and CERRA.

| Coordinates | $\bar{v}_{\mathbf{ERA5}}$ [m/s] | $\bar{v}_{\mathbf{CERRA}}$ [m/s] | $\sigma_{\mathbf{ERA5}}$ [m/s] | $\sigma_{\mathbf{CERRA}}$ [m/s] | r |
|---|---|---|---|---|---|
| 39.00°N, 13.00°E | 5.42 | 5.42 | 3.18 | 3.15 | 0.97 |
| 38.50°N, 11.75°E | 6.35 | 6.37 | 3.49 | 3.53 | 0.98 |
| 41.00°N, 11.50°E | 6.06 | 6.07 | 3.42 | 3.53 | 0.97 |
| 40.00°N, 6.75°E | 6.86 | 6.75 | 3.65 | 3.66 | 0.98 |
| 38.50°N, 18.50°E | 6.92 | 6.93 | 3.34 | 3.29 | 0.97 |

Table 3.1: Wind speed statistics comparison between ERA5 and CERRA at 100 m for offshore locations.

At the coastal site, as shown in Figure 3.3, more pronounced differences are observed between the two datasets, both in terms of mean values and variability.

CERRA presents a slightly higher monthly variability, shown by larger error bars, which suggests it captures local effects better, such as coastal orographic gradients, surface roughness and sea–land breezes. ERA5, on the other hand, has a smoother temporal profile, with lower variability and slightly higher wind speeds during winter.

These differences are mostly due to its coarser spatial resolution, which tends to smooth out small scale features near the coast.

Still, the two datasets are in very good agreement overall, the Pearson correlation around 0.95 confirms that they describe very similar wind patterns despite their differences. The table 3.2 shows the mean wind speed and standard deviation for both datasets.

As also reported by Ridal et al. [17], CERRA demonstrates a clear added value compared to the global ERA5 reanalysis, particularly in regions characterized by complex terrain or coastal influences, where the higher spatial resolution allows for a more accurate representation of near-surface variables.

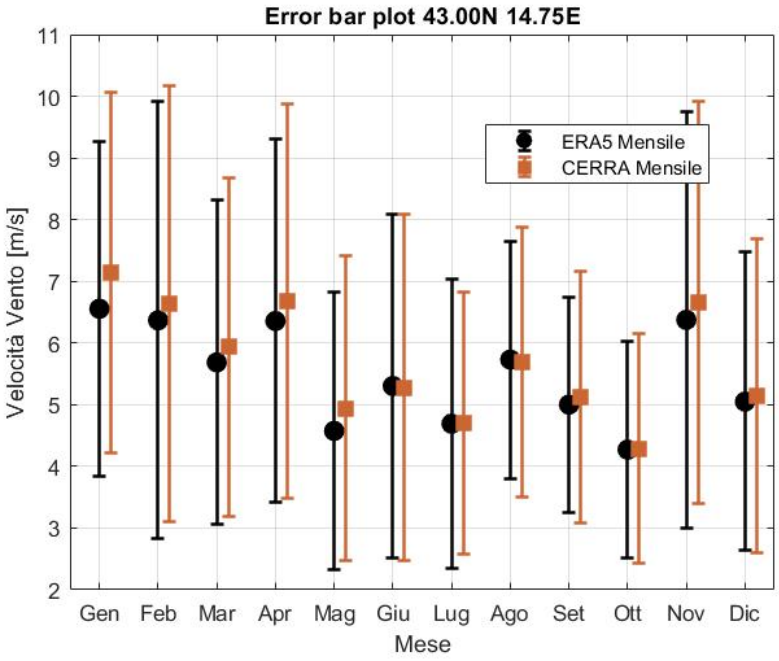


Figure 3.3: Errore bar plot at 100 for costal location.

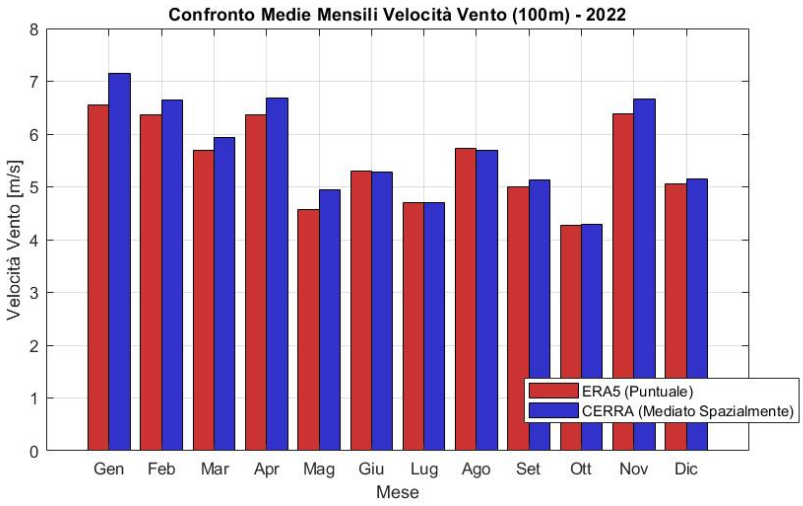


Figure 3.4: Average wind speed at 100 m for ERA5 and CERRA.

| Coordinates | $\bar{v}_{\mathbf{ERA5}}$ [m/s] | $\bar{v}_{\mathbf{CERRA}}$ [m/s] | $\sigma_{\mathbf{ERA5}}$ [m/s] | $\sigma_{\mathbf{CERRA}}$ [m/s] | r |
|---|---|---|---|---|---|
| 41.25°N, 12.50°E | 5.03 | 5.28 | 2.62 | 2.49 | 0.95 |
| 37.00°N, 16.00°E | 5.89 | 6.31 | 2.99 | 2.81 | 0.95 |
| 42.50°N, 14.75°E | 5.15 | 5.33 | 2.57 | 2.80 | 0.93 |
| 44.00°N, 13.25°E | 5.01 | 5.50 | 2.21 | 2.41 | 0.92 |
| 39.75°N, 10.00°E | 5.06 | 5.20 | 2.70 | 2.90 | 0.95 |

Table 3.2: Wind speed statistics comparison between ERA5 and CERRA at 100 m for coastal locations.

After evaluating the differences in wind speed, the analysis now focuses on the comparison between ERA5 and CERRA in terms of Annual Energy Production.This step aims to assess how the differences observed in the wind speed datasets translate into variations in the estimated energy yield.

By applying the models described in 2.4, the AEP was calculated for each site using both reanalyses, allowing a direct evaluation of their impact on energy estimation and the overall consistency between the two sources.

In the following section, several representative results are presented and discussed to highlight the main trends and differences between the datasets.

| Coordinates | AEP ERA5 [MWh/y] | AEP CERRA [MWh/y] | Difference [%] |
|---|---|---|---|
| 38.50°N, 10.50°E | 243.27 | 245.71 | +0.99% |
| 39.50°N, 13.75°E | 151.62 | 147.25 | -2.96% |
| 40.00°N, 7.75°E | 186.68 | 187.17 | +0.26% |
| 41.00°N, 11.50°E | 162.88 | 162.10 | -0.48% |
| 39.50°N, 19.00°E | 240.30 | 251.18 | +4.33% |

Table 3.3: Comparison of AEP between ERA5 and CERRA at 100 m for the selected locations.

The AEP comparison between ERA5 and CERRA shows an overall good agreement across the analyzed offshore locations.

For most case, the difference between the two datasets remains within a few percentage points, confirming the consistency already observed in the wind speed analysis at 100 m. In particular, the central offshore areas display the smallest deviations, with differences often below 2%, indicating that both reanalyses provide similar estimates of the energy potential in open sea conditions. Larger discrepancies are instead found near the coastline, where CERRA generally reports lower AEP values, due to its higher spatial resolution.

Overall, the results confirm that both datasets are highly consistent in offshore regions, while CERRA's finer resolution introduces more variability in nearshore zones, leading to slightly higher local differences in AEP.

### 3.1.2 Dataset comparison at 300 m

At 300 m height, ERA5 data were extrapolated from the 100 m level using the power law equation 2.2, while CERRA values were directly taken from its native dataset.

The comparison offshore shows that CERRA generally exhibits slightly lower mean wind speeds and larger monthly variability, while ERA5 provides a smoother profile with higher values, particularly during winter months, as shown in Figure 3.5.

Compared to the 100 m analysis, the agreement between the datasets slightly decreases at this height, yet remains very strong overall, with a Pearson correlation coefficient of 0.97. This confirms that both reanalyses provide highly consistent wind speed trends, even when extrapolating ERA5 data to upper atmospheric levels. In table 3.4 are shown wind speed statistics for the two datasets.

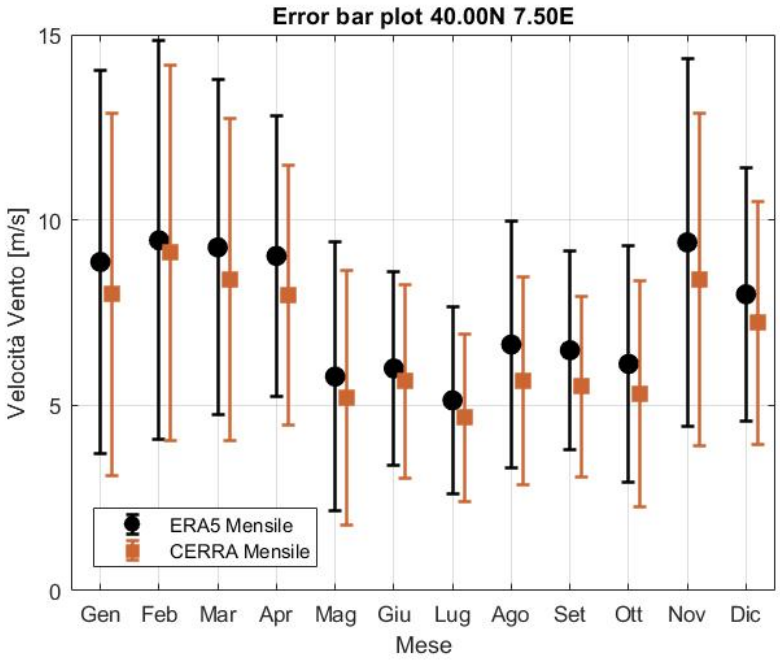


Figure 3.5: Errore bar plot at 300 m for offshore location.

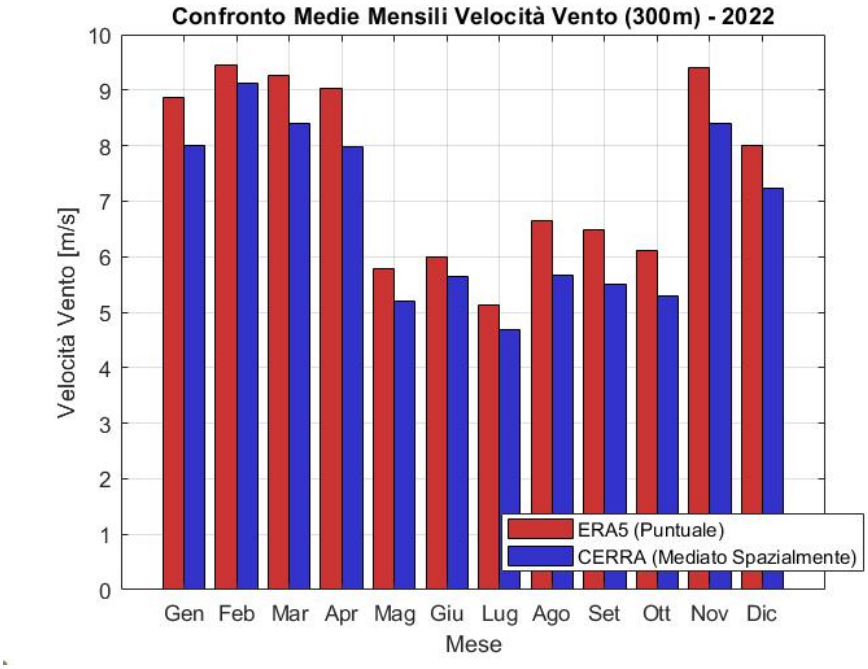


Figure 3.6: Average wind speed at 100 m for ERA5 and CERRA.

| **Coordinates** | $\bar{v}_{\mathbf{ERA5}}$ **[m/s]** | $\bar{v}_{\mathbf{CERRA}}$ **[m/s]** | $\sigma_{\mathbf{ERA5}}$ **[m/s]** | $\sigma_{\mathbf{CERRA}}$ **[m/s]** | **r** |
|---|---|---|---|---|---|
| 39.00°N, 13.00°E | 6.32 | 5.70 | 3.71 | 3.50 | 0.96 |
| 38.50°N, 11.75°E | 7.41 | 6.77 | 4.07 | 3.95 | 0.97 |
| 41.00°N, 11.50°E | 7.07 | 6.45 | 3.99 | 3.71 | 0.97 |
| 40.00°N, 6.75°E | 8.00 | 7.28 | 4.26 | 4.07 | 0.97 |
| 38.50°N, 18.50°E | 8.07 | 7.45 | 3.90 | 3.62 | 0.97 |

Table 3.4: Wind speed statistics comparison between ERA5 and CERRA at 300 m for offshore locations.

In nearshore location, the monthly wind speed profiles show slightly higher values for ERA5 throughout most of the year, whereas CERRA tends to capture more variability and lower averages, especially during the summer months. This behaviour is consistent with CERRA's higher spatial resolution, which allows it to better represent nearshore dynamics and coastal wind gradients.

When compared to the offshore site, the agreement between the two datasets slightly decreases, with a Pearson correlation in the range of 0.90 and 0.95 instead of 0.97, reflecting the greater spatial complexity typical of coastal areas.

Nevertheless, the overall correlation remains quite strong, confirming that both reanalyses provide consistent wind speed patterns even in regions where local effects are more

pronounced.

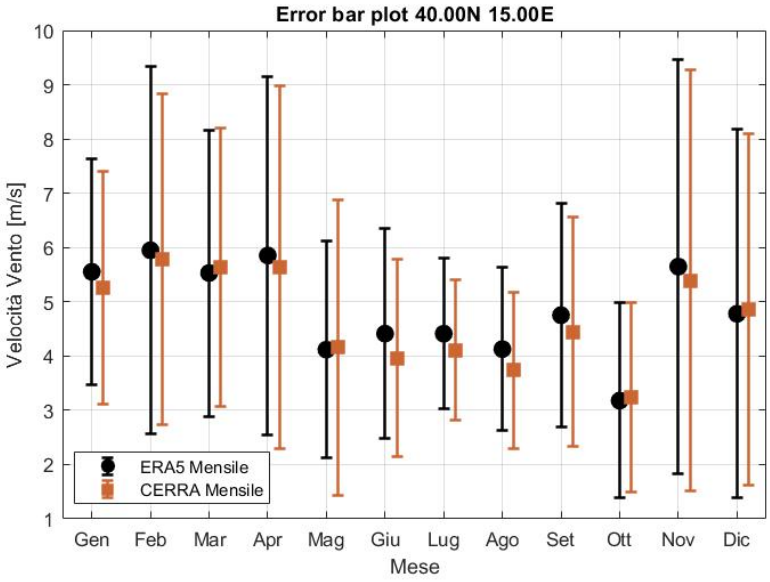


Figure 3.7: Errore bar plot at 300 for costal location.

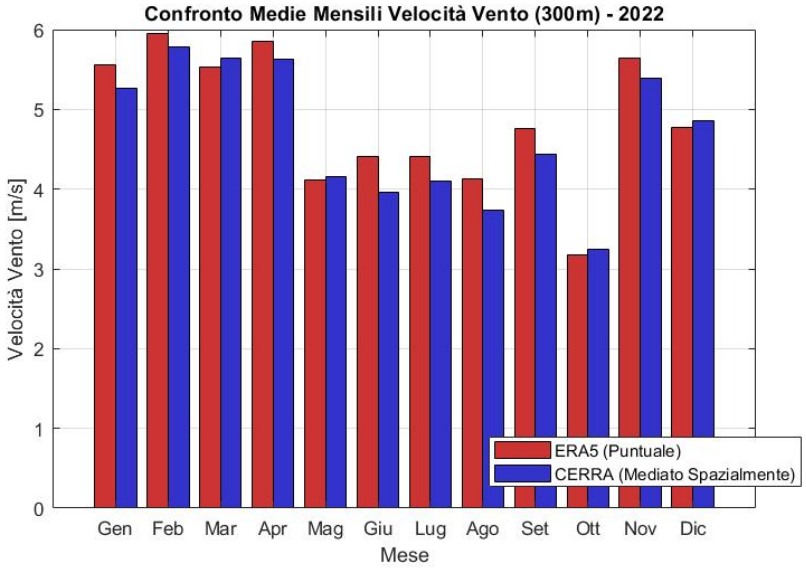


Figure 3.8: Average wind speed at 100 m for ERA5 and CERRA.

| Coordinates | $\bar{v}_{\mathbf{ERA5}}$ [m/s] | $\bar{v}_{\mathbf{CERRA}}$ [m/s] | $\sigma_{\mathbf{ERA5}}$ [m/s] | $\sigma_{\mathbf{CERRA}}$ [m/s] | r |
|---|---|---|---|---|---|
| 41.25°N, 12.50°E | 5.86 | 5.45 | 3.05 | 2.78 | 0.93 |
| 37.00°N, 16.00°E | 6.86 | 6.59 | 3.49 | 3.19 | 0.93 |
| 42.50°N, 14.50°E | 5.29 | 5.19 | 2.68 | 2.85 | 0.90 |
| 44.00°N, 13.00°E | 5.56 | 5.42 | 2.49 | 2.58 | 0.90 |
| 39.75°N, 10.00°E | 5.90 | 5.37 | 3.15 | 3.10 | 0.95 |

Table 3.5: Wind speed statistics comparison between ERA5 and CERRA at 300 m for coastal locations.

The AEP estimation process was then repeated at 300 m height to evaluate how the results change with altitude.

This additional analysis allows us to assess the consistency of the two reanalyses also at higher altitudes, where wind conditions are generally stronger and less influenced by surface effects. By comparing the resulting AEP values, it is possible to identify how the different vertical structures of the datasets affect the overall estimates of energy production.

| Coordinates | AEP ERA5 [MWh/y] | AEP CERRA [MWh/y] | Difference [%] |
|---|---|---|---|
| 38.50°N, 10.50°E | 272.04 | 243.53 | -11.71% |
| 39.50°N, 13.75°E | 181.72 | 155.17 | -17.11% |
| 40.00°N, 7.75°E | 225.82 | 196.11 | -15.15% |
| 41.00°N, 11.50°E | 218.24 | 186.68 | -16.91% |
| 39.50°N, 19.00°E | 285.86 | 259.51 | -10.16% |

Table 3.6: Comparison of AEP between ERA5 and CERRA at 300 m for the selected locations.

At 300 m height, the comparison between ERA5 and CERRA shows larger discrepancies compared to the analysis performed at 100 m.

ERA5 consistently provides higher AEP values, with differences ranging mostly between 9% and 25%. This systematic overestimation can be attributed to the extrapolation process applied to ERA5 data, which tends to amplify wind speed and, consequently, the energy yield at higher altitudes.

CERRA, on the other hand, provides slightly lower AEP estimates, likely due to its finer spatial resolution and direct representation of vertical wind profiles, which better capture the real wind shear and turbulence effects.

Despite these deviations, the two datasets maintain similar spatial trends, confirming that both reanalyses describe coherent wind and energy patterns even at higher altitudes.

Overall, the results suggest that while the extrapolated ERA5 values may introduce some bias at 300 m, both datasets remain consistent in depicting the general offshore energy potential.

## 3.2 AEP results

As expected from the comparative analysis of the two wind datasets and in agreement with the methodological discussion presented in Section 3.1, differences emerge between the results obtained from ERA5 and CERRA data.

The following sections summarize and visualize the computed AEP results for the year 2022, 2023 and 2024, using both reanalysis datasets and for two reference heights, 100 m and 300 m. Each dataset is represented by two figures displayed side by side: a spatial map of AEP density across the Italian seas and the corresponding histogram of AEP distribution per grid cell.

Those results confirm and reinforce the findings of the earlier analysis, showing the same systematic differences between the two datasets. The consistency of these divergences across independent calculations increases confidence in the robustness of the comparison and highlights the distinct behaviour of ERA5 and CERRA when applied to offshore wind assessment.

### 3.2.1 Results for 2022

**ERA5 – 100 m** The mean AEP per airborne system was estimated at 169.17 MWh/year, yielding a total offshore potential of approximately 337.11 TWh/year. Figure 3.9 illustrates the spatial distribution of AEP density and the frequency histogram for this configuration.

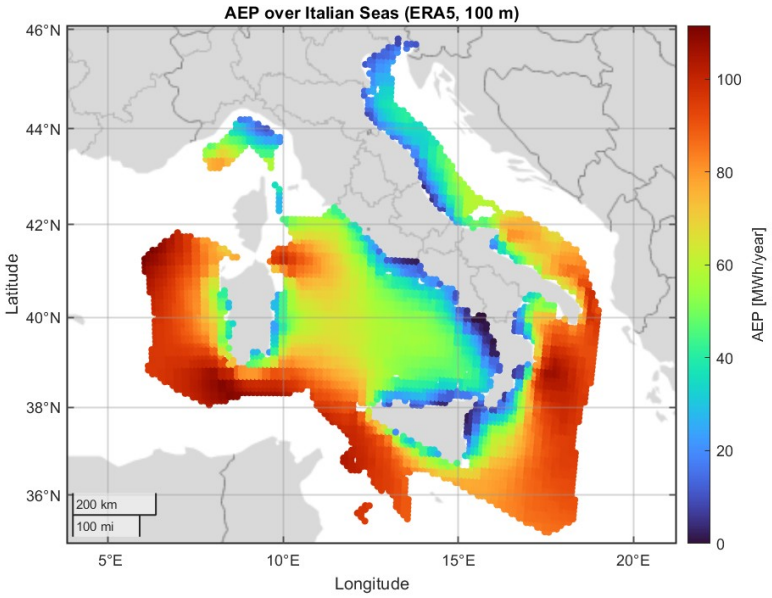


(a) AEP density map – ERA5 at 100 m (2022).

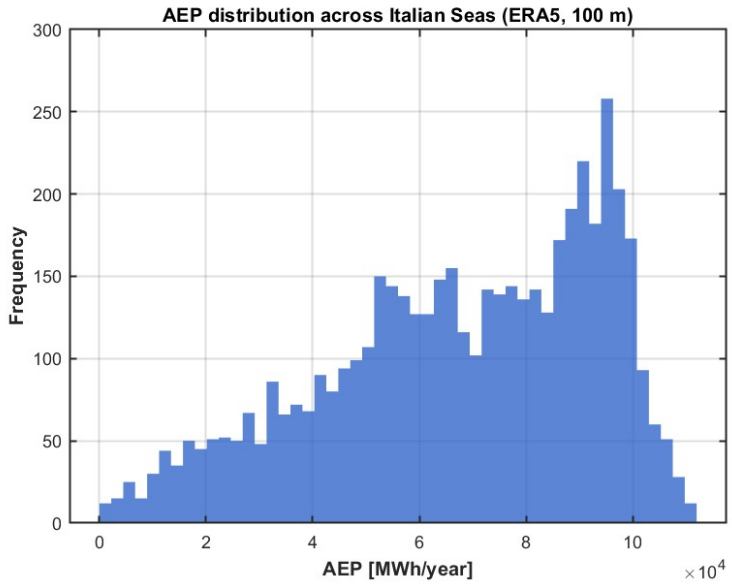


(b) AEP histogram – ERA5 at 100 m (2022).

Figure 3.9: AEP distribution for ERA5 dataset at 100 m height in 2022.

**CERRA – 100 m** For the CERRA dataset at 100 m, the mean AEP per unit reached 179.65 MWh/year, with a total estimated potential of 358.01 TWh/year. Figure 3.10 illustrates the spatial distribution of AEP density and the frequency histogram for this configuration.

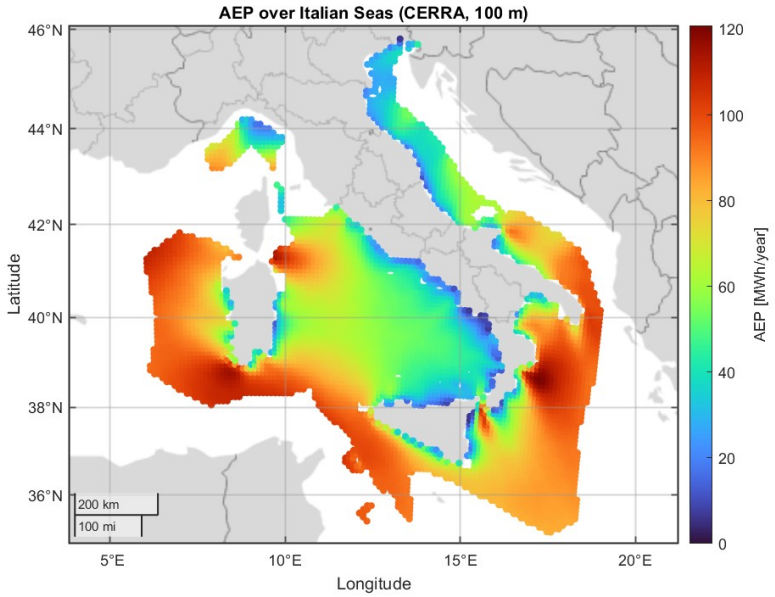


(a) AEP density map – CERRA at 100 m (2022).

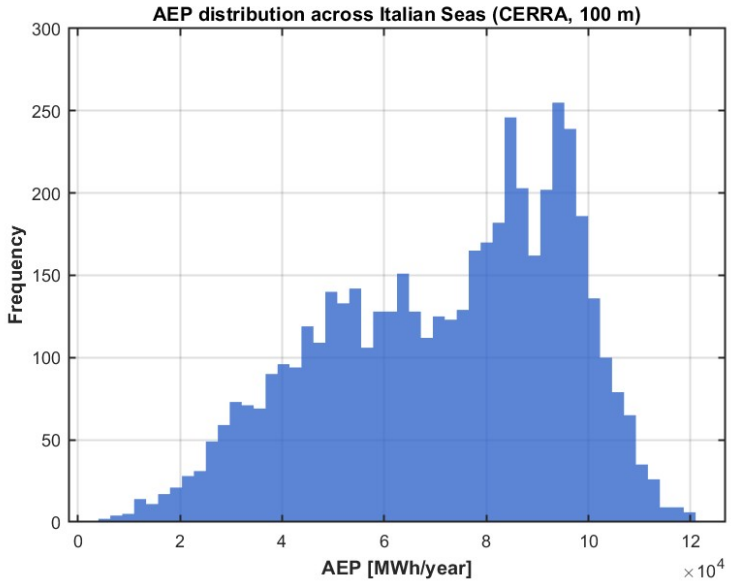


(b) AEP histogram – CERRA at 100 m (2022).

Figure 3.10: AEP distribution for CERRA dataset at 100 m height in 2022.

**ERA5 – 300 m** The ERA5 based analysis produced a mean AEP of 234.89 MWh/year, corresponding to a total offshore energy potential of approximately 468.09 TWh/year. Figure 3.10 illustrates the spatial distribution of AEP density and the frequency histogram for this configuration.

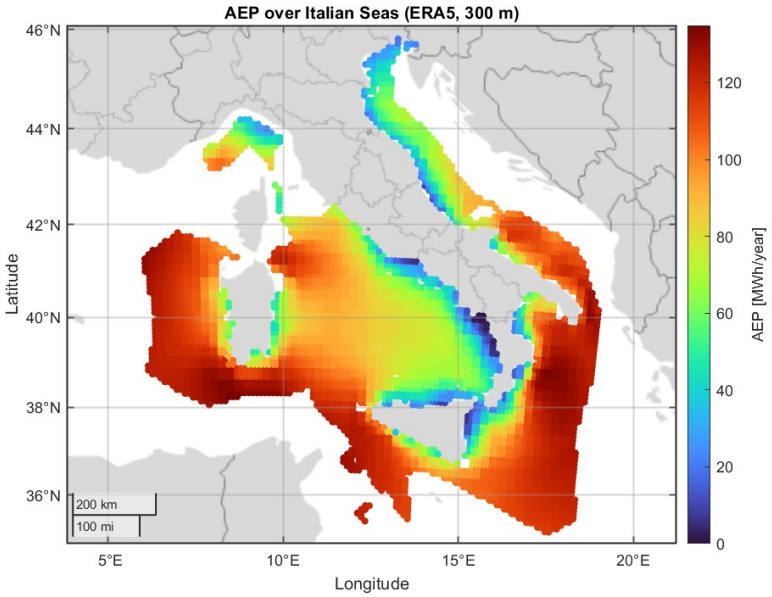


(a) AEP density map – ERA5 at 300 m (2022).

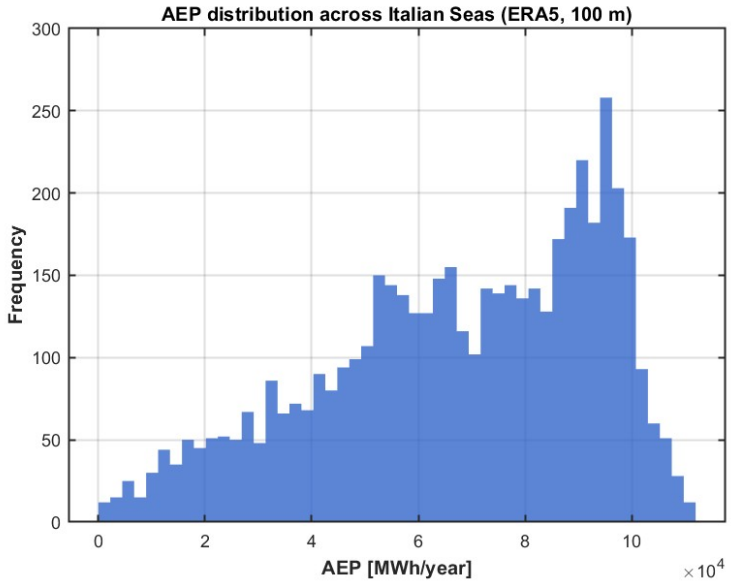


(b) AEP histogram – ERA5 at 300 m (2022).

Figure 3.11: AEP distribution for ERA5 dataset at 300 m height in 2022.

**CERRA – 300 m** The corresponding CERRA-based evaluation at 300 m resulted in a mean AEP of 204.44 MWh/year, with a total of 407.41 TWh/year. Figure 3.12 illustrates the spatial distribution of AEP density and the frequency histogram for this configuration.

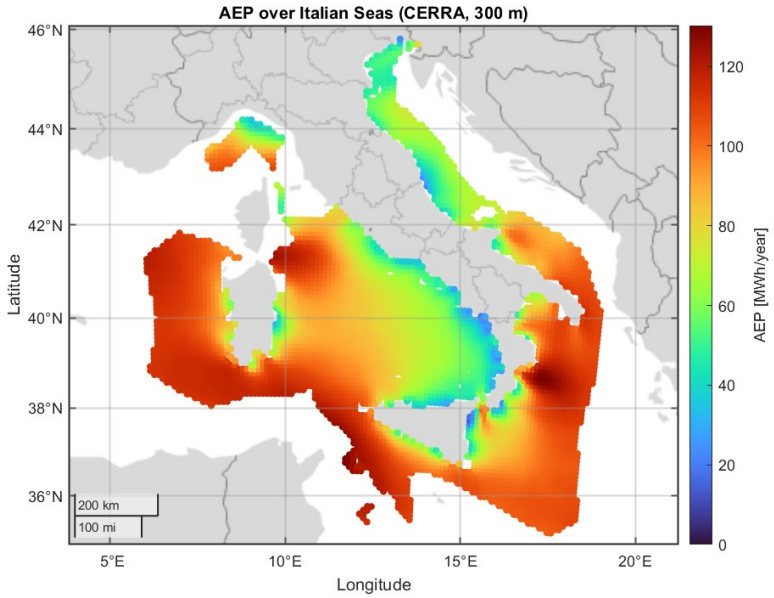


(a) AEP density map – CERRA at 300 m (2022).

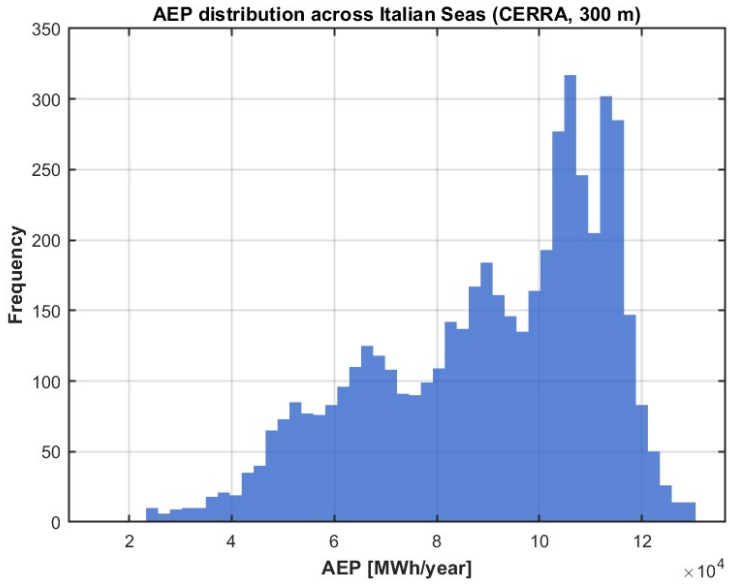


(b) AEP histogram – CERRA at 300 m (2022).

Figure 3.12: AEP distribution for CERRA dataset at 300 m height in 2022.

### 3.2.2 Results for 2023

**ERA5 – 100 m** For the year 2023, the mean AEP per airborne system was estimated at approximately 184.76 MWh/year, corresponding to a total offshore potential of around 368.19 TWh/year. Figure 3.13 illustrates the spatial distribution of AEP density and the frequency histogram for this configuration.

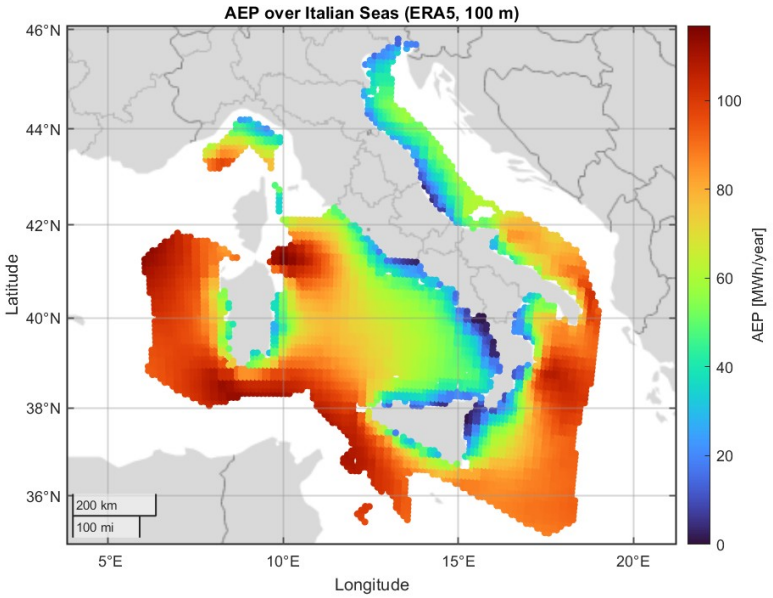


(a) AEP density map – ERA5 at 100 m (2023).

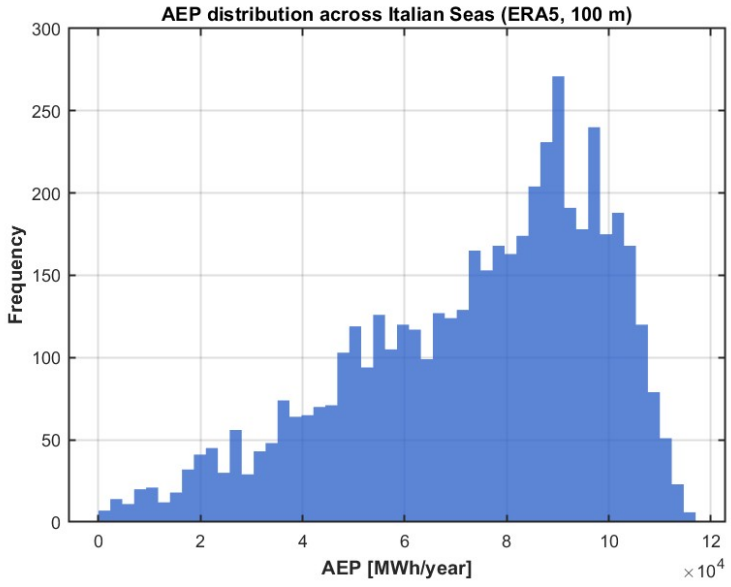


(b) AEP histogram – ERA5 at 100 m (2023).

Figure 3.13: AEP distribution for ERA5 dataset at 100 m height in 2023.

**CERRA – 100 m** For the CERRA dataset at 100 m, the mean AEP per unit reached 199.36 MWh/year, yielding a total of approximately 397.28 TWh/year. Figure 3.14 illustrates the spatial distribution of AEP density and the frequency histogram for this configuration.

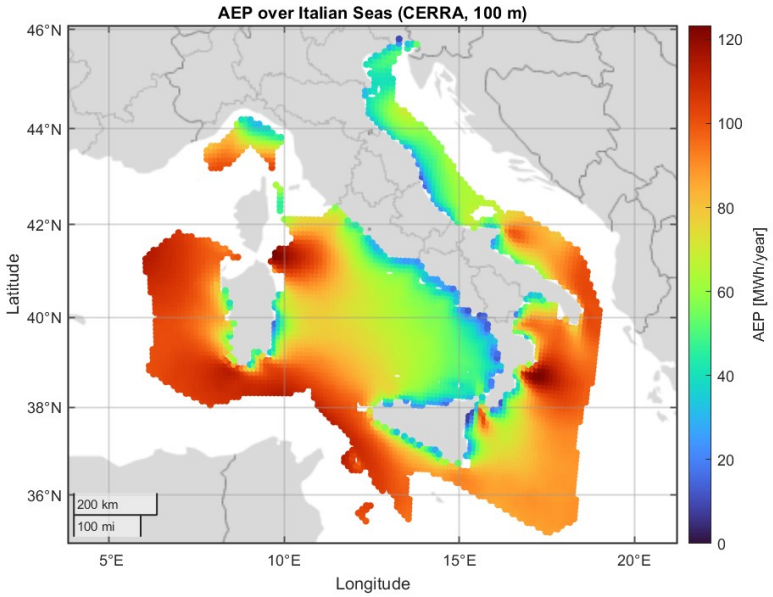


(a) AEP density map – CERRA at 100 m (2023).

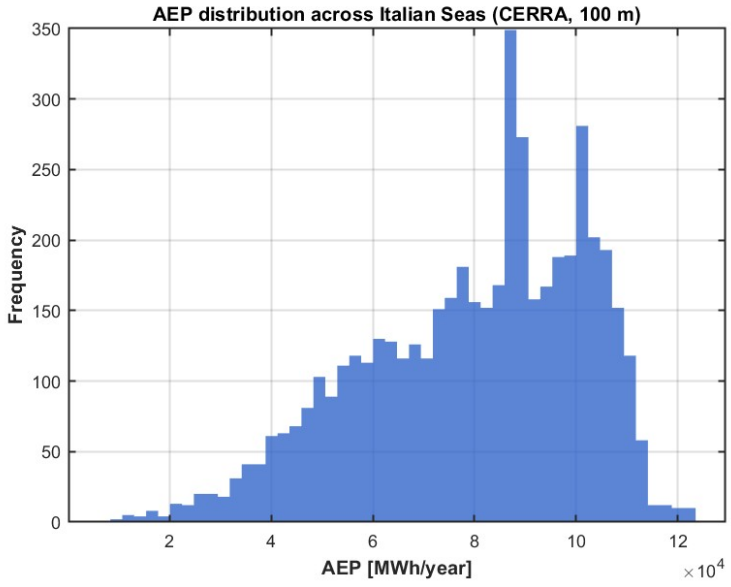


(b) AEP histogram – CERRA at 100 m (2023).

Figure 3.14: AEP distribution for CERRA dataset at 100 m height in 2023.

**ERA5 – 300 m** At 300 m, the ERA5-based computation yielded a mean AEP of 249.23 MWh/year, resulting in a total potential of approximately 496.66 TWh/year. Figure 3.15 illustrates the spatial distribution of AEP density and the frequency histogram for this configuration.

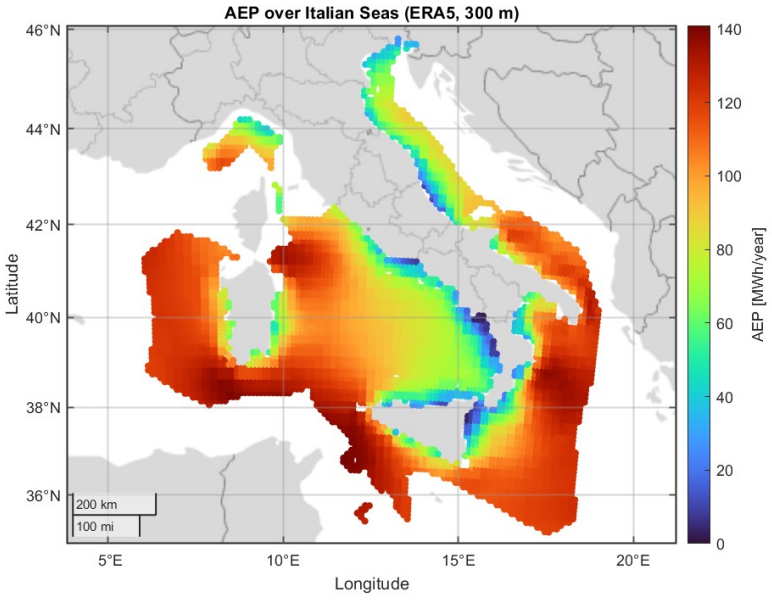


(a) AEP density map – ERA5 at 300 m (2023).

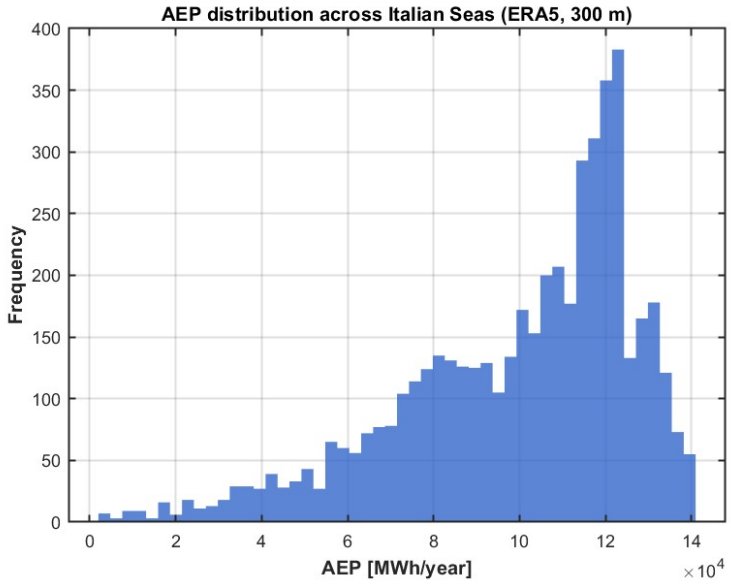


(b) AEP histogram – ERA5 at 300 m (2023).

Figure 3.15: AEP distribution for ERA5 dataset at 300 m height in 2023.

**CERRA – 300 m** For the CERRA dataset, the analysis at 300 m indicated a mean AEP of 225.59 MWh/year, with a total energy potential of approximately 449.56 TWh/year. Figure 3.16 illustrates the spatial distribution of AEP density and the frequency histogram for this configuration.

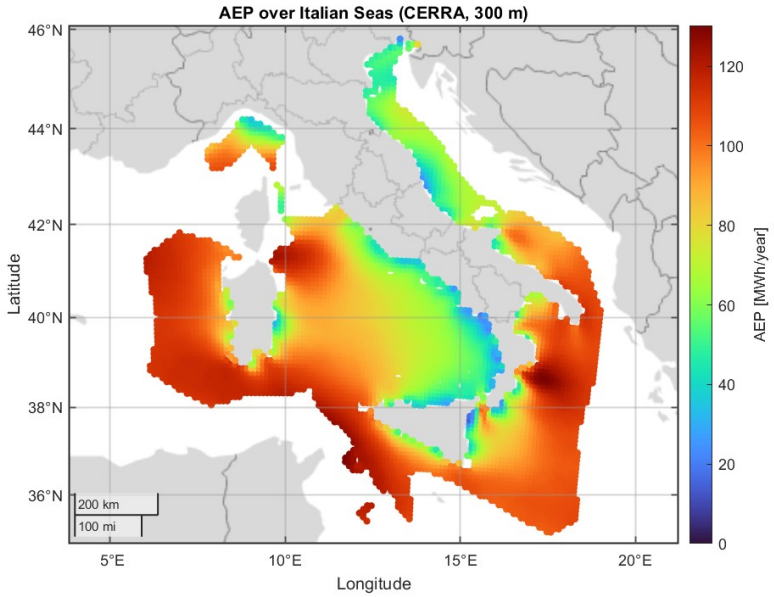


(a) AEP density map – CERRA at 300 m (2023).

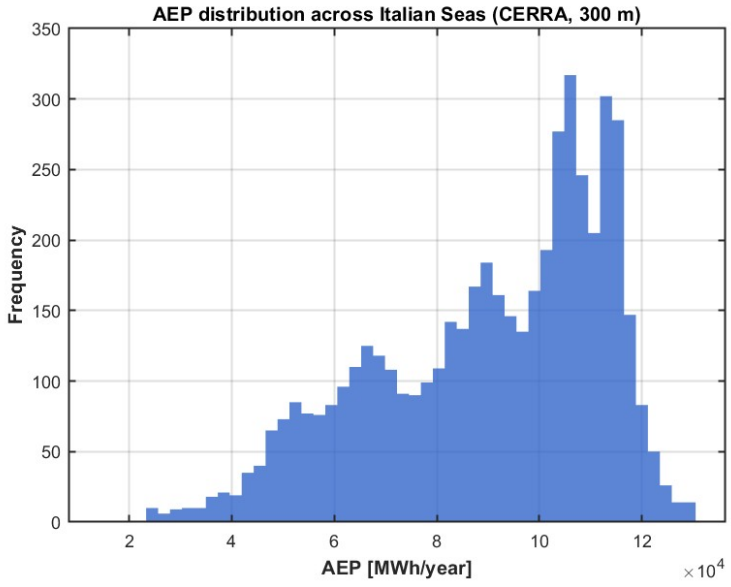


(b) AEP histogram – CERRA at 300 m (2023).

Figure 3.16: AEP distribution for CERRA dataset at 300 m height in 2023.

### 3.2.3 Results for 2024

**ERA5 – 100 m** The mean AEP for system obtain is 177.64 MWh/year, leading to a total offshore potential of about 354.00 TWh/year. Figure 3.17 illustrates the spatial distribution of AEP density and the frequency histogram for this configuration.

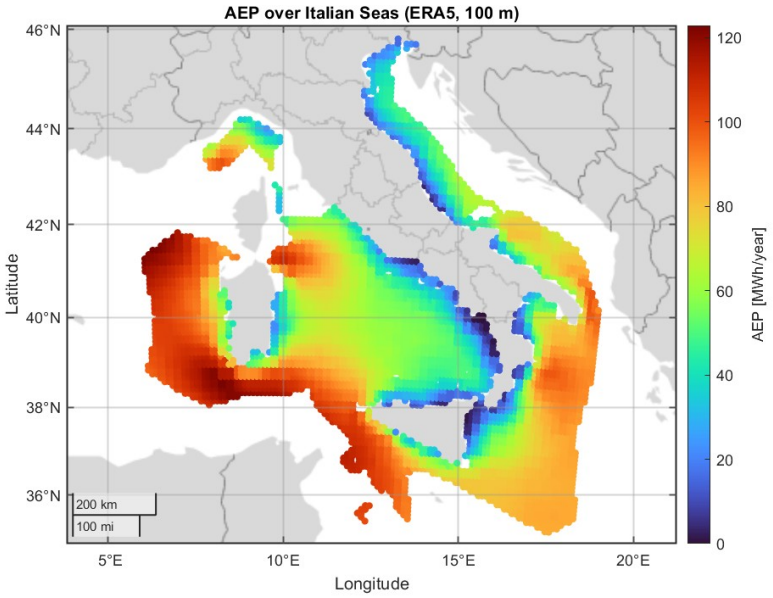


(a) AEP density map – ERA5 at 100 m (2024).

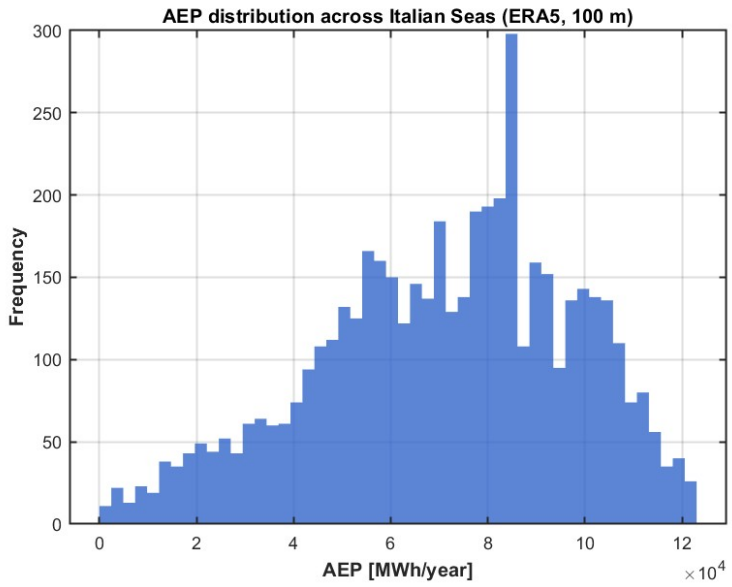


(b) AEP histogram – ERA5 at 100 m (2024).

Figure 3.17: AEP distribution for ERA5 dataset at 100 m height in 2024.

**CERRA – 100 m** At 100 m, the CERRA dataset produced a mean AEP per system of 179.43 MWh/year, corresponding to a total potential of approximately 357.57 TWh/year. Figure 3.18 illustrates the spatial distribution of AEP density and the frequency histogram for this configuration.

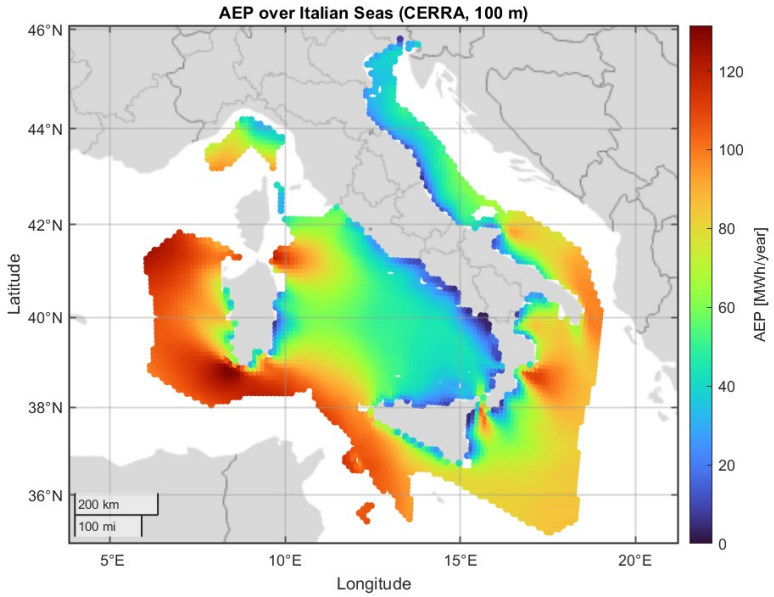


(a) AEP density map – CERRA at 100 m (2024).

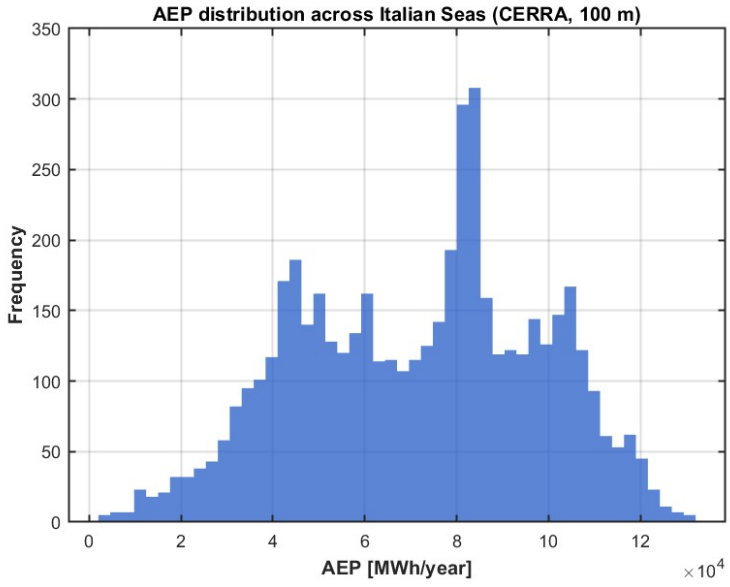


(b) AEP histogram – CERRA at 100 m (2024).

Figure 3.18: AEP distribution for CERRA dataset at 100 m height in 2024.

**ERA5 – 300 m** At 300 m, the ERA5-derived mean AEP increased to 244.82 MWh/year, yielding a total estimated potential of 487.88 TWh/year. Figure 3.19 illustrates the spatial distribution of AEP density and the frequency histogram for this configuration.

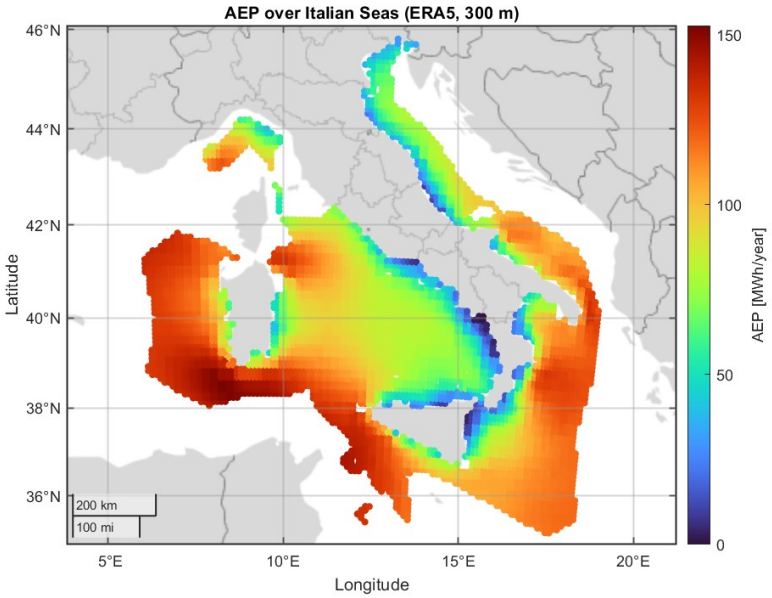


(a) AEP density map – ERA5 at 300 m (2024).

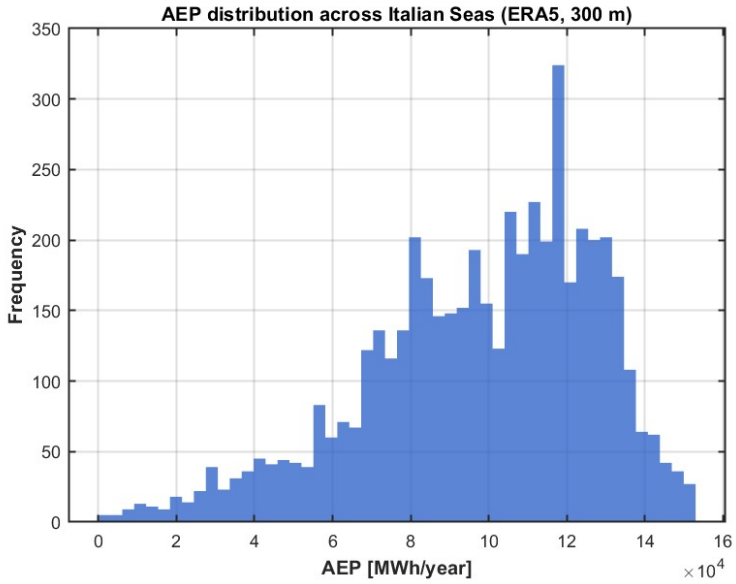


(b) AEP histogram – ERA5 at 300 m (2024).

Figure 3.19: AEP distribution for ERA5 dataset at 300 m height in 2024.

**CERRA – 300 m** Finally, the CERRA dataset at 300 m yielded a mean AEP of 209.68 MWh/year, leading to a total estimated offshore potential of approximately 417.85 TWh/year. Figure 3.20 illustrates the spatial distribution of AEP density and the frequency histogram for this configuration.

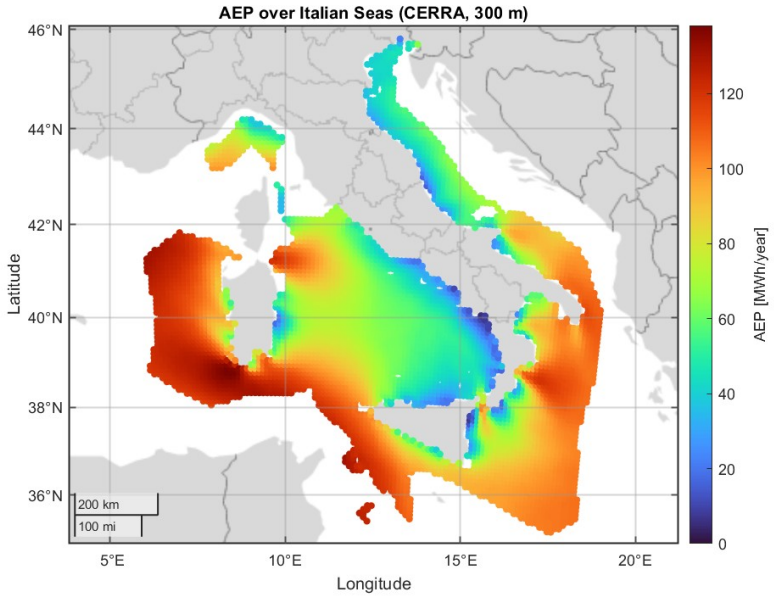


(a) AEP density map – CERRA at 300 m (2024).

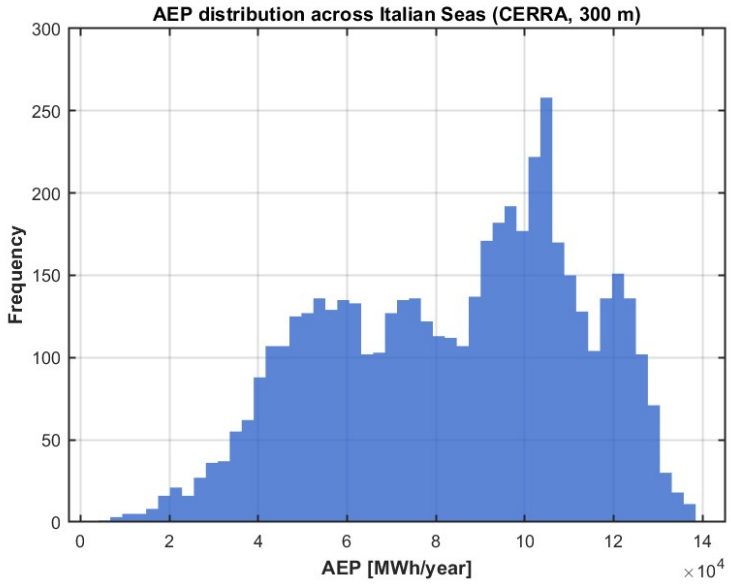


(b) AEP histogram – CERRA at 300 m (2024).

Figure 3.20: AEP distribution for CERRA dataset at 300 m height in 2024.

### 3.2.4 Results comparison

In the following tabe are collected all the results previously shown.

| Dataset | Height [m] | Year [–] | Mean AEP [MWh/y] | Offshore Potential [TWh/y] |
|---|---|---|---|---|
| ERA5 | 100 | 2022 | 169.17 | 337.11 |
| ERA5 | 300 | 2022 | 234.09 | 468.09 |
| ERA5 | 100 | 2023 | 184.76 | 368.19 |
| ERA5 | 300 | 2023 | 249.23 | 496.66 |
| ERA5 | 100 | 2024 | 177.64 | 354.00 |
| ERA5 | 300 | 2024 | 244.82 | 487.88 |
| CERRA | 100 | 2022 | 179.65 | 358.01 |
| CERRA | 300 | 2022 | 204.44 | 407.41 |
| CERRA | 100 | 2023 | 199.36 | 397.28 |
| CERRA | 300 | 2023 | 225.59 | 449.56 |
| CERRA | 100 | 2024 | 179.43 | 357.57 |
| CERRA | 300 | 2024 | 209.68 | 417.85 |

Table 3.7: Mean AEP and total offshore potential for ERA5 and CERRA across the analysed years.

The analysis of the Annual Energy Production results over multiple years and different heights shows that both ERA5 and CERRA describe similar spatial and temporal patterns. In both cases, the strongest wind potential is found in the Tyrrhenian Sea while Adriatic and Ionian ones show lower average values, with these trends remaining constant for the three years considered.

Looking at table 3.7 is it possible to see that the mean AEP values per machine in between 170 and 185 MWh/y at 100 meter above ground, while at 300 meter this value is between 235 and 250 MWh/y.

The estimation at 100 m is comparable between the two dataset, while at 300 m ERA5 and CERRA present some differences where ERA5 is likely to report higher values of AEP with respect to the CERRA ones. This differences confirms what already discussed in section 3.1.

## 3.3 Consideration

Placing the obtained AEP estimates within Italy's current and projected electricity demand provide a clear measure of AWE's potential and relevance.

According to TERNA [25], the national electricity consumption in 2022 amounted at

the valure of 316.5 TWh. In comparison, the offshore AWE potential al 300 m reaches values higher than 400 TWh, depending on the dataset selected and reference year. This means that, under the appropriate assumptions, the theoretical potential of airborne wind systems offshore could theoretically equal or exceed Italy's present electricity demand, highlighting their significance as a large scale renewable resource.

Looking ahead, ISPRA's projections for 2050 foresee national electricity consumption ranging from about 260 TWh in high-efficiency scenarios up to around 450 TWh in strongly electrified pathways involving widespread heat pump and electric vehicle adoption. Within these ranges, the modeled AEP potential would still represent a substantial share of future national demand, confirming the strategic importance of offshore wind and, by extension, airborne systems in supporting Italy's energy transition.

Despite these promising results, several limitations must be acknowledged when interpreting the modeled AEP values. The simulations include the operational wind range defined by cut-in and cut-out speeds, but they do not account for system downtime related to maintenance operations, component eplacement, or unexpected failures. In reality, such interruptions would reduce the effective Annual Energy Production, meaning that the results presented here should be interpreted as idealized upper-bound values rather than realistic operational outputs.

Additionally, the analysis assumes that AWE systems could be theoretically deployed over the entire offshore domain considered. In practice, however, such full area installation is not technically, economically, or environmentally feasible. Marine spatial planning constraints, conflicts with navigation routes, fisheries, and protected areas, as well as installation and maintenance costs, would significantly limit the actual deployable surface and the corresponding energy yield. Therefore, the results quantify a theoretical resource potential, not the achievable installed capacity.

Summing up, this study indicates that offshore AWEy systems hold a considerable renewable energy potential for Italy, with a production magnitude comparable to the Italy's current annual electricity demand. This indicates that, at a purely theoretical level, the offshore AWE resource could cover a role as a strategic component of Italy's future renewable energy portfolio. Nevertheless, translating this theoretical potential into actual deployment will depend on technological improvements, cost competitiveness and supportive regulatory conditions.

In the following chapter the focus is placed on the economic dimension, specifically addressing the Levelized Cost of Energy analysis to evaluate the cost-effectiveness of offshore AWE systems.

# 4 | Economic Analysis

To fully assess the potential of an emerging technology, it is not sufficient to estimate its energy yield alone; it is equally important to evaluate its position within the energy market and determine whether it can be considered competitive with existing technologies. For this purpose, the most widely adopted and comparable indicator is the Levelized Cost of Energy. It provides a single, comparable metric that indicates the minimum selling price required for the project to break even.

Currently, the reference techno-economic model for Airborne Wind Energy systems was developed by Rishikesh Joshi, designed specifically to estimate the LCoE of a single tethered wing system operating onshore. In this work, the model has been taken as a baseline and adapted, as far as possible given the limited data available, to represent the characteristics and cost structure of Offshore Airborne Wind Energy systems in Italy.

## 4.1 LCoE definition

The Levelized Cost of Energy is the most commonly used metric for comparing the economic performance of different energy technologies. It represents the average cost of producing one unit of electricity over the entire project lifetime, accounting for all expenditures incurred during installation, operation and end of life activities. To provide a fair comparison across technologies and deployment conditions, both costs and energy are discounted over time according to a chosen real discount rate.

The LCoE is defined as the ratio between the discounted sum of lifetime costs and the discounted sum of net energy produced. However, for emerging technologies such as AWE, public subsidies may play a critical role in enabling early commercial deployment. To reflect these effects, the conventional formulation can be extended by incorporating the impact of capital grants or production based incentives.

The expression adopted is therefore:

$$\mathrm{LCoE} = \frac{\sum_{t=0}^{T} \frac{\mathrm{CapEx}(t) + \mathrm{OpEx}(t) - \mathrm{Subsidy}(t)}{(1+r)^t}}{\sum_{t=0}^{T} \frac{\mathrm{AEP}(t)}{(1+r)^t}}. \tag{4.1}$$

Where:

- CapEx($t$): capital expenditure in year $t$. In most projects it's entirely concentrated at $t = 0$, representing the initial investment;
- OpEx($t$): operational and maintenance costs incurred during year $t$, including maintenance, unscheduled repairs, leasing fees and any other yearly operating costs relevant to the technology;
- Subsidy($t$): financial support received in year $t$, modeled as a direct reduction in the effective cost of the project. This term may include upfront investment grants, feed-in premiums, production based incentives or any form of economic compensation;
- $r$: real discount rate used to discount future costs and energy production, reflecting the time value of money as well as project specific financial risk;
- $T$: total project lifetime expressed in years. Typical values range between 20 and 30 years for energy technologies;
- AEP($t$): net Annual Energy Production in year $t$, after accounting for losses (availability, electrical losses, wake effects if present, etc.). This represents the effective delivered energy contributing to project revenues.

## 4.2 Reference cost model

The cost model adopted in this thesis is based on the reference techno-economic framework developed by R. Joshi [12] and later refined through a collaborative process involving AWES companies, tether and ground-station manufacturers, component suppliers and academic institutions. The resulting model, released as an open source MATLAB implementation, represents the first coordinated effort to establish a unified and transparent methodology for the economic assessment of AWES.

Its objective is to define a consistent set of cost functions and design metrics that can support both conceptual design studies and earlystage commercial evaluations. It provides

a modular set of models linking subsystem design, operational behaviour and economic performance through the LCoE. Given the limited availability of empirical data during development, the model was deliberately constrained to the analysis of a single and onshore AWE unit. By excluding offshore components and farm level interactions such as wakes, cabling or array layout, the authors were able to focus on identifying the dominant design drivers, key cost components and principal physical–economic trade-off governing system feasibility.

In the present thesis, this reference framework is adopted and extended to enable the techno-economic evaluation of offshore AWE applications. The most significant enhancement concerns the energy modelling: the simplified, non site specific AEP estimation originally used in the Joshi model has been replaced with the wind resource assessment methodology developed in the previous chapters, based on reanalysis datasets (ERA5 and CERRA) and a specific power curve. This modification allows the evaluation of site dependent offshore AEP with greater accuracy. In addition, the cost structure of the original model was expanded to account for the specific requirements of offshore and farm deployment.

### 4.2.1 Model structure

The core of Joshi's work is the development of an integrated MDAO (Multidisciplinary Design, Analysis and Optimization) framework whose comprehensive objective is the minimisation of the LCoE. It combines the competing goals of maximising energy production and minimising total system cost into a single holistic metric, providing one of the earliest systematic methodologies for evaluating the techno-economic performance of AWES.

This model decomposes the AWES into its main subsystems: tether, ground station and Balance of System (BoS), assigning specific cost functions to each component. This structure provides a transparent representation of how design choices propagate through subsystem costs and ultimately affect LCoE.

Figure 4.1 shows the breakdown of the cost components included in the model, highlighting the hierarchical organisation of components and subcomponents.

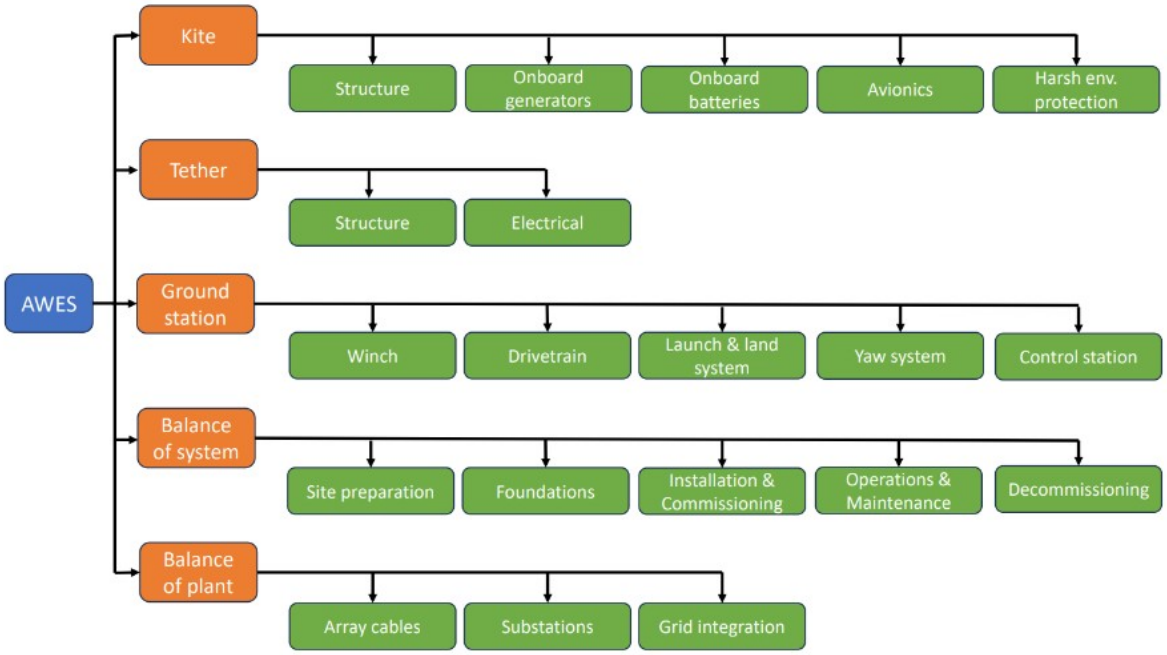


Figure 4.1: Breakdown of cost components used in the Joshi model [12]. The system in represented in 'blue', the components in 'orange' and the subcomponents in 'green'.

The cost model distinguishes between capital expenditure, operational expenditure and decomissioning costs. For each subcompnents, costs are parameterised using design variables such as wing area, tether mass or rated power, enabling a consistent evaluation across different system sizes.

**Kite System** The capital expenditure of the kite system is driven primarily by the kite mass and wing area. Mass dependent costs capture composite materials, adhesives and manufacturing processes, while area dependent costs reflect surface finishing and coatings. For operational expenditure, only the kite replacement cost is included, assuming a reference lifetime of 5000 full load flight hours. Due to the lack of reliable data, operational costs associated with auxiliary onboard components are not modelled.

**Tether** The tether is a major structural component designed to withstand the traction force. Its capital cost scales with tether mass, typically using a unit cost of approximately 80€/kg. Operational expenditure is dominated by tether replacement, because operating cyclically, tether degradation represents one of the most critical contributors. In particular bending fatigue is the primary failure mechanism in ground-generation systems and creep for flight-generation systems.

**Ground Station** The ground station houses the electrical drivetrain, electronics control and energy storage. Drivetrain components (gearbox, generator, power converters) are sized according to the rated power and the power crest factor, which determines the allowable peak-to-rated power ratio. Energy storage is necessary to smooth the oscillating power output before grid injection. In the reference model, this is achieved using ultracapacitors, whose capital cost scales linearly with the rated capacity. Operational costs arise from maintenance and periodic replacements, based on annual charge–discharge cycles compared to the manufacturer's lifetime.

**Balance of System (BoS)** The BoS includes all onshore infrastructure required to install and operate a single AWES unit. All components site preparation, foundations, installation and commissioning, O&M and decommissioning. They are all modelled as linear functions of the rated power. This simplification reflects the early stage nature of available data and ensures consistency within the parametric framework.

**Balance of Plant (BoP)** The BoP refers to farm level infrastructure such as array cabling, substations and grid interconnection. These components are not included in the original Joshi model, which is restricted to single system onshore configurations.

**Optimisation** Beyond the cost model, an essential feature of the Joshi framework is the definition of several AWES component parameters that act as independent design variables and can be tuned to minimise the LCoE.
In this thesis, the most relevant parameters are:

- Wing area: proportional to the kite size, it determines material mass, manufacturing cost and the amount of aerodynamic force the system can generate;
- Aspect ratio: influences both the aerodynamic efficiency of the wing and its structural mass, affecting lift-to-drag performance and construction requirements;
- Maximum wing loading: sets the upper limit on the aerodynamic loads that the wing can withstand, defining the maximum achievable power output and directly impacting the system's capacity factor;
- Maximum allowable tether stress: determines the required tether diameter, which affects aerodynamic drag, structural reliability and the frequency of tether replacement over the system lifetime;
- Power crest factor: defined as the ratio between the peak reel-out power and the rated generator power, it governs generator sizing and influences both dynamic

loading and cost.

A nested optimisation strategy is employed within the framework. For each design configuration defined, the operational variables are optimised to maximise the average cycle power. This approach ensures a coherent exploration of the design space and captures the strong coupling between aerodynamic performance, structural sizing and overall techno economic feasibility.

### 4.2.2 Assumptions and limitations

Due to the early stage of AWE development, the model is still characterised by significant uncertainties.

From a wind modelling perspective, the aerodynamic formulation assumes quasi steady behaviour with constant aerodynamic coefficients, without capturing unsteady effects, turbulence or detailed flight mechanics. The parameters used in the original model follow the idealised reference conditions defined by the IEC standards for wind turbine assessment. These standards specify uniform assumptions on wind statistics, turbulence intensity and operational limits in order to allow consistent performance comparisons across different wind energy technologies.

Within this framework, the model adopts wind characteristics representative of IEC Class I conditions, namely a mean wind speed of 8.5 m/s and a turbulence intensity of 0.2 at a reference height of 100 m. These values correspond to Weibull coefficients of approximately $a = 8$ m/s and $k = 2$, describing an energetic but idealised wind regime. In addition to these assumptions, the model applies simplified operational thresholds by defining fixed cut-in and cut-out wind speeds, with the upper limit capped at 25 m/s.

The Annual Energy Production is then computed from a Weibull distribution generated internally by the model and using ideal and roughly estimated power curve. For that reasons the resulting AEP tends to be optimistic and does not reflect the performance limitations of existing airborne technologies.

Also cost models are still characterised by significant uncertainty. They depend strongly on factors that are not strictly technical, such as manufacturing practices, supply chain maturity, geographical context and general market conditions. For this reason, several assumptions were necessary to construct the reference cost model, especially regarding commercial readiness and system scaling.

The cost functions presented in the reference report are based on early commercialisation scenarios, considering system sizes between 100-2000 kW and production volumes of at

least 50 units. Overhead development costs, profit margins and company specific contingencies are not included, since these elements vary greatly with technology readiness level and commercial maturity.

Although the reference cost model currently represents the most complete set of AWE specific cost functions available, it remains limited to single system configurations intended for onshore deployment. These functions rely on simplifying assumptions that reflect the scarcity of validated industrial data but is also align with the purpose of the framework, which is to provide a conceptual and computationally efficient tool as a techno-economic benchmark for AWE.

## 4.3 Model implementation

Since no full scale offshore AWE farms currently exist, there is no validated cost breakdown for such systems. In addition, there are no operational prototypes under construction and no published studies on offshore AWE farms, either in Italy or abroad. The absence of industrial deployment is reflected in the academic literature as well. For this reason, the present work represents a first attempt to develop a techno-economic assessment adjust to the Italian context, adapting existing modelling tools to the characteristics of the selected sites. Since the original model was conceived for single onshore ground-generation systems, several modifications were required to make it representative of offshore multi unit configurations. The adaptations implemented in this thesis can be grouped into two main areas: wind energy modelling and economic modelling.

### 4.3.1 Wind energy modeling

While the use of IEC style reference conditions ensures internal coherence within the conceptual framework, it does not account for the variability of site specific wind regimes or for the influence of atmospheric stability and height dependent wind profiles. These limitations restrict the applicability of the original model to realistic offshore environments and motivate the methodological extensions introduced in this thesis.

The first step of the modelling work consisted in enlarging the framework to the most appropriate atmospheric dataset in light of the analyses carried out in the previous chapters. Based on the comparative assessment of ERA5 and CERRA, the framework was designed to allow the user to specify the dataset and operative altitude. The model automatically adapts its calculations to the characteristics of the selected reanalysis product, particularly with respect to vertical resolution and the availability of wind levels, following the

procedures illustrated in sections 2.4 and 2.5.

Therefore, were implemented a series of new functions that enable the user to define the geographical position of the site through latitude and longitude, select ERA5 or CERRA, and retrieve the corresponding wind time series at the desired height. The wind data are then processed at the chosen coordinate, from which the model computes the Weibull parameters $a$ and $k$. These parameters allow the reconstruction of the local wind probability distribution, replacing the idealised and non site specific statistical assumptions used in the original framework.

At this stage, the analysis was deliberately limited to a single reference location rather than extended to a broader offshore region, expanding the dataset comparison to a spatial domain would represent a useful direction for future developments.

The energy model was also modified to incorporate the digitised power curve extracted from the verified SkySails technical datasheet [24], chosen as reference. Following the methodology presented in section 2.5, the Weibull distribution is multiplied by the power curve to obtain the pointwise AEP, which provides a representative estimate of the average energy yield of a single unit within the farm. In this phase, the operational range of the system was extended by adopting a cut-out wind speed of 25 m/s, resulting in higher production values compared to those obtained in the previous chapter.

Then the total power output of the farm is calculated as the sum of the contributions from each installed unit. The model allows the user to define the total number of airborne systems and to select different AWE technologies or configurations for comparative analyses. Once the total installed capacity is defined, the farm AEP is obtained by multiplying the single system AEP by the number of operational units.

By relying on real atmospheric datasets and a empirical power curve, the updated energy model produces AEP values that are significantly more realistic and no longer affected by the systematic overestimation of the reference framework. The resulting energy assessment provides a faithful representation of the performance that an offshore AWE system could achieve in the selected regions of the Italian seas, thereby improving the reliability of the techno economic analysis.

However, despite these improvements, the modelling work remains limited by the scarcity of validated aerodynamic and atmospheric data for airborne systems. It was not possible to account for wake interactions between neighbouring units or to parametrise turbulence intensity, since no suitable multi unit aerodynamic models or offshore turbulence datasets exist for AWES at present. These constraints prevent a rigorous optimisation of farm

layout and highlight the need for further research and experimental validation as the technology progresses.

### 4.3.2 Cost modeling

A second set of adaptations concerns the economic model. The model was expanded to include offshore specific Balance of System and Balance of Plant components, capturing the main cost categories that typically arise in marine environments.

Because no validated cost data currently exist for offshore AWE technology, these new components were formulated using cost related to offshore wind turbine farm. The main references used is the NREL cost breakdown of an offshore floating farm [26], which provides empirical cost trends in aggregated expressions, normalised per installed megawatt (€/MW) rather than detailed parametrisations.

Because the available cost data are highly aggregated, it was not possible to distinguish clearly between the costs associated with the primary energy conversion system and those related to the farm level infrastructure. As a consequence, the Balance of System costs used in this work inherently include part of the Balance of Plant expenditure, since the NREL dataset does not allow a more detailed separation of these categories. Despite this limitation, the choice was made to rely on NREL data because it represents the most robust and widely validated source currently available for offshore cost estimation, ensuring the highest degree of reliability achievable within the present level of technological maturity.

The extensions aimed to represent the key components typically included in Balance of Plant and Balance of System categories, such as foundations, electrical infrastructure, installation logistics and decommissioning.

According to NREL, the total capital expenditure for a floating offshore wind system amounts to approximately 6,169 €/kW, of which the substructure and foundation account for nearly 28%. The detailed distribution of costs is summarized in Table 4.3.2.

| Component | Category [–] | Cost [€/kW] | Share [%] |
|---|---|---|---|
| Substructure and Foundation | CapEx | 1708 | 27.7 |
| Electrical Infrastructure | CapEx | 1157 | 18.8 |
| Assembly and Installation | CapEx | 279 | 4.5 |
| Development and Project Management | CapEx | 98 | 1.6 |
| Lease Price | CapEx | 167 | 2.7 |
| Soft Costs (commissioning, finance) | CapEx | 1060 | 17.2 |
| **Total CapEx** | | **6169** | **100.0** |
| **O&M (Floating Platforms)** | OpEx | **87** | – |
| Maintenance (labour + vessels) | OpEx | 56 | – |
| Operations (admin + port fees) | OpEx | 30 | – |
| Insurance | OpEx | 15 | – |

Table 4.1: Breakdown of capital and operational costs.

The results confirm that floating substructures and their associated marine operations dominate the BoS costs, representing more than half of the total investment. In particular, substructure and foundation costs alone can exceed those of the system itself, reflecting the engineering complexity and logistical challenges of deep water installations.

All cost components listed in table 4.3.2, as well as the default cost items inherited from the original Joshi framework, are then automatically scaled according to the number of installed units. This procedure provides a first order estimation of the total capital and operational expenditures for a customizable offshore AWE farm layout, ensuring coherence between the energy yield assessment and the economic model.

The adapted framework was not intended for optimisation, but rather for producing a realistic preliminary estimate of the total project cost and the corresponding LCoE. For this reason, configurations that were not compatible with the characteristics of the selected offshore site or with the available technological constraints were not considered.

The resulting model therefore bridges the gap between single system AWE design and offshore wind farm economics. Although simplified, it captures the main cost drivers and functional dependencies required to evaluate the economic feasibility of offshore AWE projects under the conditions relevant to the Italian seas.

### 4.3.3 Case study definition

Because the available cost data for offshore AWE technology are extremely limited and do not allow the parametrisation of offshore cost functions for optimisation, this study adopts a reference approach based on an existing offshore wind farm project. The objective is to place the techno-economic assessment within a realistic geographical and infrastructural context, while maintaining a scale compatible with the current maturity level of AWE technology.

As a reference site, this work uses the offshore area associated with the Med Wind project in the Sicilian Channel, approximately 60 km west of the Sicilian coastline and more than 12 nautical miles from the Egadi Islands. The site is characterised by water depths ranging from 100 m to nearly 900 m, which makes fixed bottom foundations unfeasible and therefore requires floating substructures.

The Med Wind project, currently under environmental evaluation, foresees the installation of roughly 190 floating wind turbines rated at 14.7 MW each, for a total capacity of about 2.8 GW. The plant is divided into three offshore sub fields, each connected to an offshore transformer module and to the mainland grid via high voltage direct current export cables. Once completed, it would be the largest floating wind farm in Europe, with an estimated annual production of more than 8.4 TWh and a capacity factor of around 34% [15, 19].

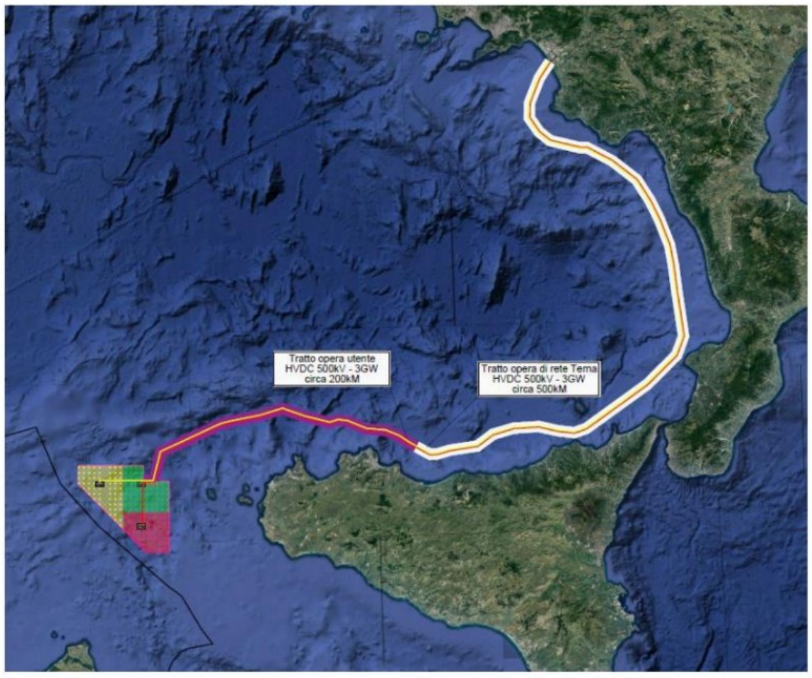


Figure 4.2: Med Wind farm site [19].

Although highly informative for understanding offshore project scale and layout in the central Mediterranean, such dimensions are not representative of the current development stage of airborne wind systems. AWE units have significantly lower rated power, much higher technological uncertainty and no existing offshore prototypes from which to derive validated farm design principles. For this reason, a reduced scale offshore AWE farm is defined in the present study, maintaining the same geographical area but adjusting it to a size compatible with near term deployment of airborne systems.

To determine the number of AWE units that could be realistically installed in that area, the total Med Wind offshore surface was divided into square cells with side length equal to twice the tether length. Each square represents the operational flight window of a single AWE system, ensuring sufficient clearance to avoid tether crossings. The number of deployable units obtained from this geometric partition was then divided by a factor of two to approximate the reduction in usable area caused by wake effects. This procedure yields a total of 1211 AWE systems that can operate within the considered offshore area under simplified spacing assumptions.

This approach provides a base model that is consistent with real offshore spatial constraints while remaining compatible with the scale and technological maturity of AWE systems. It also allows direct comparison between AWE and conventional offshore wind projects operating under similar site conditions, offering a meaningful reference for the subsequent techno economic evaluation.

The base case assumes the following parameters [24]:

| Parameter | Symbol / Unit | Base Case Value |
|---|---|---|
| Kite area | $N$ [m$^2$] | 150 |
| Tether length | $L$ [m] | 500 |
| Tether diameter | $d$ [mm] | 14 |
| Rated power per AWE unit | $P_{\text{unit}}$ [kW] | 100 |
| Number of AWE units | $N$ [-] | 1211 |
| Total installed capacity | $P_{\text{farm}}$ [MW] | 121.1 |
| Project lifetime | $n$ [y] | 25 |
| Discount rate | $r$ [%] | 7.8 |
| Reference wind height | $H$ [m] | 300 |
| Reference dataset | – | CERRA 2024 |
| Cost model references | – | Joshi [12], NREL [26] |

Table 4.2: Input parameters and assumptions for the offshore AWE base case scenario.

The adaptations described above define the structure of the base offshore AWE model used in this study, providing a coherent framework for evaluating the techno economic performance of a representative early stage offshore deployment.

Building upon this reference configuration, the following chapter presents the results obtained for the base case and explores a set of sensitivity analyses designed to quantify the influence of key design parameters.

# 5 | Results of Economic Analysis

## 5.1 Overview

This chapter presents the Levelized Cost of Energy results for the reference of offshore AWE farm defined in section 4.3.3, considering the design parameters reported in table 4.2.

The first analysis regard two baseline cases: a single machine configuration and a farm scale deployment. Then, a series of sensitivity analysis is presented to evaluate how key parameters influence the overall cost of energy. These include variations in tether length, operating reference height and the introduction of policy incentives such as CapEx based subsidies. Together, these scenarios provide an overview of the techno-economic performance of the system and highlight the main factors affecting its competitiveness in offshore environments.

### 5.1.1 Base case: Single AWE

The following table reports the baseline techno-economic results for a single 100 kW offshore AWE unit operating at the selected reference height. Annual Energy Production, capacity factor and the resulting LCoE are computed using both ERA5 and CERRA datasets for the range of years 2022-2024, in order to quantify the impact of dataset choice on performance and cost metrics.

| Dataset | Year [-] | CF [–] | $AEP_{unit}$ [MWh/y] | CapEx [k€] | OpEx [k€/y] | LCoE [€/MWh] |
|---|---|---|---|---|---|---|
| ERA5 | 2022 | 0.41 | 357.96 | 640 | 18 | 215 |
| ERA5 | 2023 | 0.44 | 388.67 | 640 | 19 | 201 |
| ERA5 | 2024 | 0.44 | 386.54 | 640 | 19 | 203 |
| CERRA | 2022 | 0.35 | 310.24 | 640 | 17 | 245 |
| CERRA | 2023 | 0.39 | 341.43 | 640 | 18 | 226 |
| CERRA | 2024 | 0.39 | 332.10 | 640 | 18 | 231 |

Table 5.1: Base case results for a single AWE using ERA5 and CERRA (2022-2024).

In the following figures 5.1 and 5.2 are presented the detailed 2024 costs breakdown.

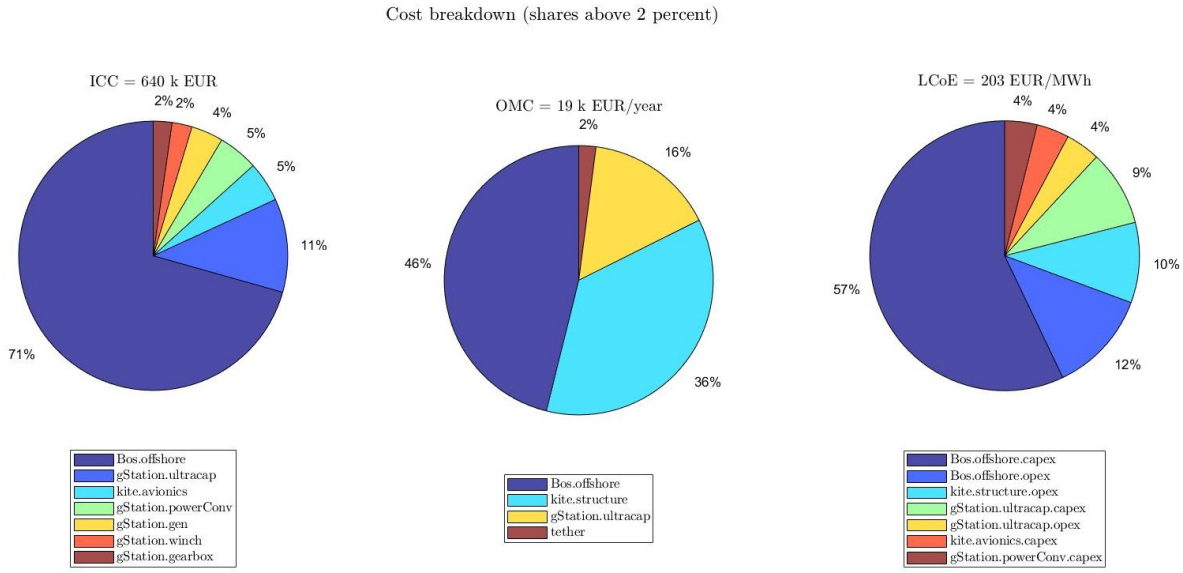


Figure 5.1: ERA5 cost breakdown for 2024.

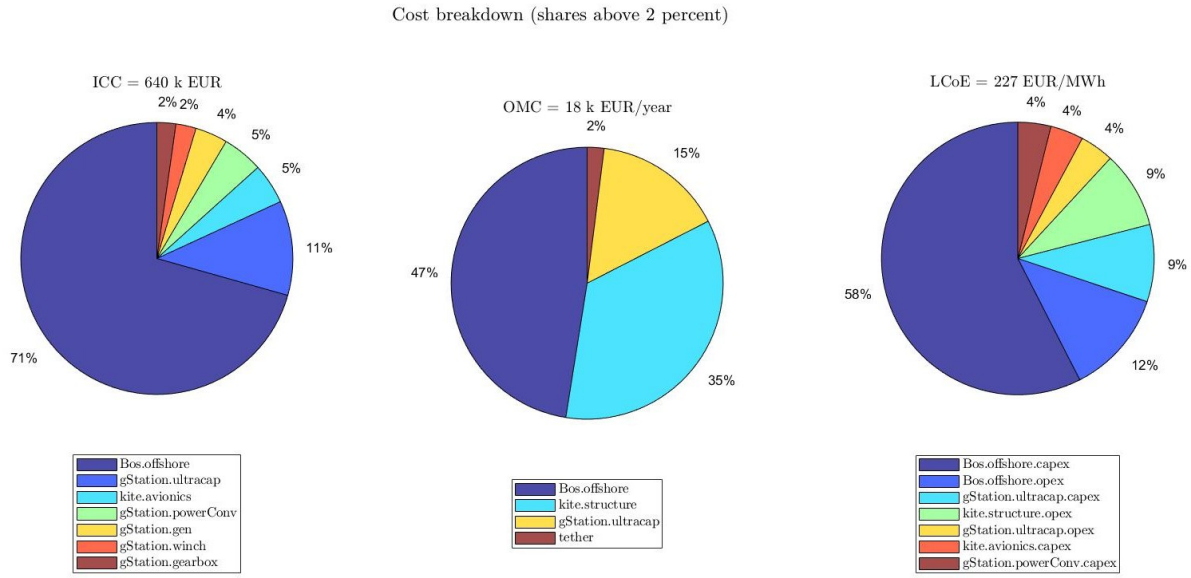


Figure 5.2: CERRA cost breakdown for 2024.

The results reflect the behaviour already observed in previous parts of this research: ERA5 systematically yields higher wind speeds at mid altitude compared to CERRA. This is largely due to the way ERA5 reconstructs vertical wind layers through model extrapolation, which tends to overestimate the available resource at higher altitudes. Conversely, CERRA, with its finer spatial resolution and more conservative vertical wind profile, provides lower wind speed estimatation.

These differences directly propagate into the energy yield. ERA5 produces higher AEP values of 358–389 MWh/y and capacity factors of 0.41–0.44, resulting in lower LCoE values of 201–215 €/MWh for the single machine configuration. CERRA, on the other hand, results in AEP values of 310–341 MWh/y and capacity factor values between 0.35 and 0.39, leading to higher LCoE values equal to 226–245 €/MWh. Since CapEx of 640 k€ and OpEx of 17–19 k€/y remain constant across all scenarios, the LCoE differences arise entirely from the variability of the dataset used in energy production. This reinforces the conclusion that wind resource uncertainty at operational altitude remains one of the major contributors to AWE techno-economic variability.

When comparing the techno-economic performance of the analysed offshore AWE unit with the cost benchmarks reported in the NREL cost of wind energy review [26], the differences in maturity and scale become explicit. The AWE system exhibits, when expressed in specific terms (M€/MW), a capital cost of 6.4 M€/MW and operational expenditures of 170–190 k€/MW/y, resulting in LCoE values between 201 and 245 €/MWh depending

on the wind dataset used. By contrast, NREL reports a representative floating offshore wind turbine (12 MW) with a CapEx of 6.17 M€/MW, OpEx of 87 k€/MW/y and an LCoE around 140 €/MWh . Although the specific CapEx of the AWE unit is remarkably close to that of a commercial scale floating turbine, the corresponding OpEx is roughly two times higher, reflecting the early stage nature of AWE technology and the absence of economies of scale. These higher operational costs, combined with the substantially lower rated power and energy output, explain the significantly higher LCoE observed for AWE.

### 5.1.2 Base case: Farm AWE

To assess the effect of scaling, the analysis is extended to a large AWE farm configuration, constructed by replicating the reference unit and deploying 1211 devices within a predefined offshore area. The objective is not to optimise spatial layout but to quantify how much the implementation would cost.

The following table presents the costs adapted to the farm layout.

| **Dataset** | **Year** [–] | **CF** [–] | **AEP$_{unit}$** [MWh/y] | **Total AEP** [GWh/y] | **CapEx** [k€] | **OpEx** [€/y] | **LCoE** [€/MWh] |
|---|---|---|---|---|---|---|---|
| ERA5 | 2022 | 0.41 | 357.96 | 433.50 | 775166 | 21695 | 215 |
| ERA5 | 2023 | 0.44 | 388.67 | 470.68 | 775166 | 23008 | 201 |
| ERA5 | 2024 | 0.44 | 386.54 | 464.47 | 775166 | 22840 | 203 |
| CERRA | 2022 | 0.35 | 310.24 | 375.75 | 775166 | 20763 | 245 |
| CERRA | 2023 | 0.39 | 341.43 | 413.48 | 775166 | 22188 | 226 |
| CERRA | 2024 | 0.39 | 332.10 | 411.29 | 775166 | 21688 | 231 |

Table 5.2: Base case results for an AWE farm using ERA5 and CERRA (2022–2024).

The transition from a single AWE unit to a fullbscale offshore farm does not significantly modify the techno-economic behaviour. As shown in Table 5.2, capacity factors and AEP$_{unit}$ values replicate the same dataset-dependent pattern observed in the single machine analysis, with ERA5 consistently yielding higher performance than CERRA. As a consequence, the farm LCoE remains confined to essentially the same interval (approximately 200-245€/MWh), indicating that the current cost model does not yet capture meaningful economies of scale in shared offshore infrastructure, installation, or O&M logistics. This outcome is fully consistent with the modelling assumptions adopted, which exclude farm-level synergies or shared-infrastructure savings.

This result becomes particularly evident when comparing the theoretical farm output of the reference wind farm, the Med Wind project, which is projected to generate approximately 10.5 TWh/y. By contrast, an AWE-based farm of equal spatial extent equipped with 100 kW units would produce only a small fraction of this energy, despite the large number of devices, due to the intrinsically lower rating of current AWE systems. The comparison highlights how the absence of MW-scale AWE machines remains a primary limiting factor for large scale offshore deployment and prevents AWE farms from competing with established floating-wind projects in terms of total annual production.

To better interpret LCoE differences we report the detailed cost breakdown distribution in Figure 5.3 and Figure **??**.

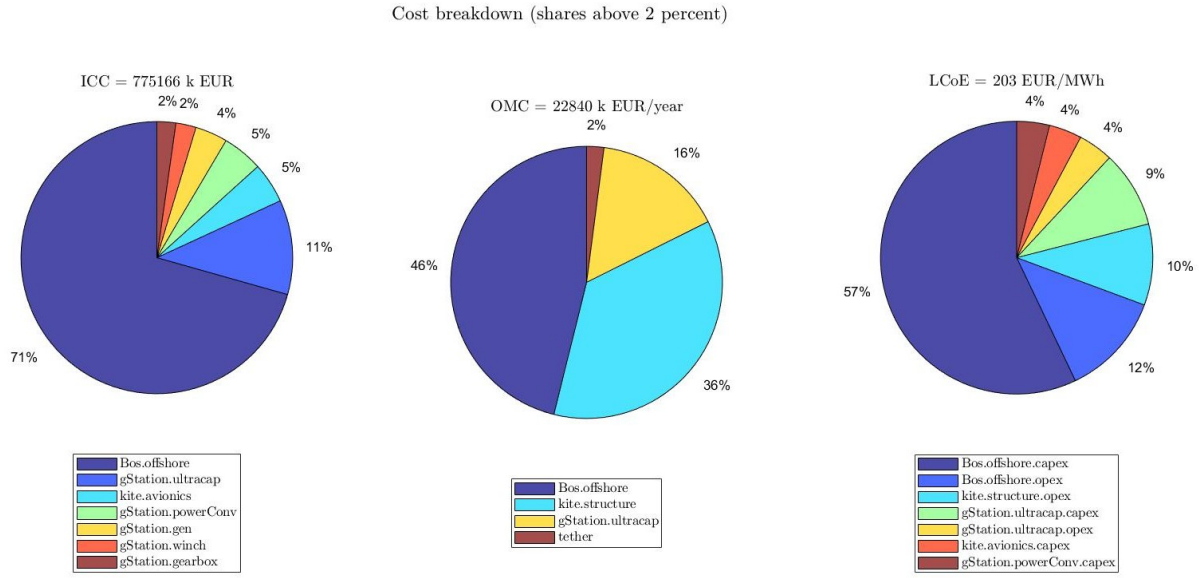


Figure 5.3: ERA5 cost breakdown for 2024.

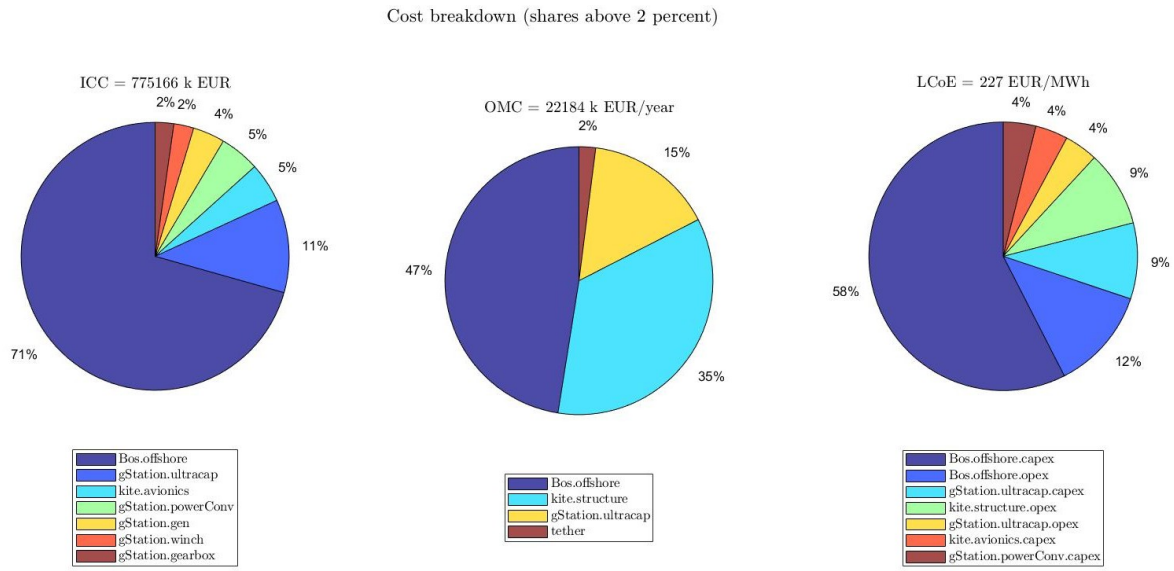


Figure 5.4: CERRA cost breakdown for 2024.

For both datasets, CapEx is overwhelmingly dominated by the offshore Balance of System, which accounts for roughly 70% of the total investment. The remaining 30% is distributed across the kite structure, ultracapacitors, avionics, power conversion and generator systems, each contributing only a few percent. The OpEx displays a similar pattern, infact operational costs related to offshore has the largest share, followed by maintenance of the kite structure and the ultracapacitor subsystem.

This distribution closely mirrors that of a traditional floating offshore wind farm. In commercial floating wind, 50–70% of total CapEx typically comes from offshore infrastructure (floating platform, moorings, installation, export cable), while turbine-specific components represent the remaining fraction. Similarly, OpEx is largely driven by offshore operations and maintenance, with smaller shares allocated to component upkeep.

It should be noted that, in the present study, several installation and infrastructure cost categories could not be modelled using proper scaling laws due to the limited availability of validated offshore AWE data. This limitation implies that the resulting CapEx and OpEx values are likely overestimated compared to what would be obtained with a fully scalable cost model calibrated on real offshore AWE deployments.

## 5.2 Sensitivity Analysis

To complement the evaluation of the base case, a sensitivity analysis was carried out to investigate how variations in selected technical and economic parameters influence the

resulting LCoE. Given the early development stage of offshore airborne wind systems, the sensitivity analysis serves as a crucial tool to assess the robustness of the results and to identify potential pathways for cost reduction and performance improvement. All variations were performed with respect to the 2024 base case computed using the CERRA dataset, which was chosen as reference due to its higher accuracy at elevated operating heights.

### 5.2.1 Operating Height

As tether materials, control strategies and airborne structures evolve, it is reasonable to expect that longer and more reliable tethers will enable operation at increasingly higher altitudes. Accessing these higher layers of the atmosphere may provide stronger and more stable wind conditions, thus improving both energy yield and economic performance.

In this context, the analysis examines how the AEP and LCoE change when operating at 300 m, 400 m and 500 m. The results are reported in the following table 5.3.

| **Height [m]** | **$AEP_{unit}$ [MWh/y]** | **CF [-]** | **LCoE[€/MWh]** |
|---|---|---|---|
| 300 | 339.63 | 0.39 | 227 |
| 400 | 337.62 | 0.39 | 227 |
| 500 | 330.26 | 0.38 | 231 |

Table 5.3: Sensitivity S1: operating height.

The results show that increasing the operating height from 300 m to 500 m does not lead to higher energy production. Both AEP and capacity factor remain almost unchanged and the associated LCoE differs only marginally. Although higher altitudes are often expected to provide stronger and more consistent winds, the atmospheric structure above coastal and offshore regions explains the limited benefits observed here.

Several observational studies show that wind speed tends to stabilise beyond a certain height, remaining nearly unchanged above roughly 250-300 m. This behaviour is consistent with the results obtained in the present analysis, where the AEP at 400 m does not differ significantly from the value computed at the reference height of 300 m.

The slight decrease in AEP observed at higher operating altitudes is therefore unlikely to be caused by a reduction in wind speed itself, and is more plausibly attributed to the atmospheric mechanisms described below.

LiDAR measurements by Sakagami et al. [21] reveal that the wind speed can remain nearly constant with height around 300 m during periods of low wind shear and may even slightly decrease above 240-300 m under stable marine conditions. Such behaviour is linked to reduced turbulent momentum mixing and increased atmospheric stratification in the upper part of the marine boundary layer.

Similarly, Banta et al. [2] showed that coastal and offshore environments often develop low-level wind maxima within the 100–300 m layer, followed by flattened or even declining wind profiles at higher altitudes due to enhanced atmospheric stability and weaker turbulent mixing.

As a result, operating an AWE system at 400 m or 500 m does not yield stronger winds than at 300 m, which explains the very small differences in AEP, CF and LCoE across the analysed heights.

### 5.2.2 Tether length

In this sensitivity analysis, the effect of tether length on system costs is examined. The tether diameter is fixed at 14 mm, so variations arise purely from changes in total cable length. Increasing the tether length enables the AWE system to reach higher operating altitudes, potentially accessing stronger or more persistent winds. However, this aerodynamic benefit comes at the expense of higher material, installation and maintenance costs, which scale directly with the total tether length.

| L [m] | CapEx [€] | OpEx [€/y] |
|---|---|---|
| 500 | 9163 | 367 |
| 600 | 10996 | 440 |
| 700 | 12828 | 513 |
| 800 | 14661 | 587 |

Table 5.4: Sensitivity S1: effect of tether length on LCoE.

The results show a clear, almost linear increase in both CapEx and OpEx as the tether length extends from 500 m to 800 m. CapEx rises from 9163€ to 14661€ due to the proportional growth in material and manufacturing costs, while OpEx increases from 367€/y to 587€/y because longer tethers require more extensive inspection, experience greater mechanical loading and are exposed to higher cumulative wear.

Longer tethers make it possible to reach higher operating altitudes however, this benefit does not automatically translate into improved techno-economic performance. As high-

lighted by Joshi et al. [12], AWE system design is governed by several competing scaling trends, where increases in tether length and mass introduce additional structural loads, higher drag, growing material and maintenance costs. These effects can counteract or even outweigh the aerodynamic advantages attained at higher altitude.

Therefore, the optimal operating height results from a balance between the potential energy production gains offered by higher winds and the economic penalties associated with deploying longer and heavier tethers [12].

Although longer tethers are not economically favourable in the present configuration, they remain essential for enabling access to higher atmospheric layers. Should they prove beneficial under different site conditions or future technological developments. At present, the added cost, mass and drag associated with longer lines outweigh the limited wind speed gains, but this balance may shift. Advances in tether materials, aerodynamic optimisation and larger AWE system designs could reduce these penalties and make higher altitudes more attractive.

For this reason, maintaining the possibility of operating with longer tethers has strategic value, as it broadens the future operating envelope of AWE systems and prepares the technology for scenarios in which higher altitudes become energetically advantageous.

### 5.2.3 Policy incentives

To evaluate the potential impact of investment based policy support on the economic performance of offshore Airborne Wind Energy systems, a sensitivity analysis was conducted by applying a capital grant to the initial investment cost. The incentive considered reflects the 40% CapEx grant mechanism adopted in national funding schemes for renewable energy projects. In particular, the measure under PNRR [9] provides a non repayable contribution up to 40% of admissible investment costs for new renewable energy installations in energy community configurations. The table below reports the resulting CapEx, OpEx, and LCoE variations for grant levels of 20% and 40%, compared to the baseline case without incentives.

| Scenario | CapEx [k€] | OpEx [k€/y] | LCoE [€/MWh] | ΔLCoE [%] |
|---|---|---|---|---|
| Baseline | 775166 | 22184 | 227 | - |
| CapEx Grant 20% | 620133 | 22184 | 193 | -15% |
| CapEx Grant 40% | 465100 | 22184 | 158 | -30% |

Table 5.5: Sensitivity S3: effect of investment grants.

The results indicate that applying a CapEx grant has a strong effect on improving the economic performance of the offshore AWE system. Even modest support reduces the LCoE noticeably and a 40% capital grant brings a substantial improvement in cost competitiveness. This behaviour is expected for small scale, capital intensive technologies where upfront investment dominates the LCoE structure.

When compared with mature floating offshore wind systems, however, the AWE unit remains considerably more expensive. According to NREL's Cost of Wind Energy Review [26], commercial floating offshore wind farms operate with CapEx around 6.17 M€/MW, OpEx near 87 k€/MW/y and LCoE values of 135–145 €/MWh. Even after applying investment support, the AWE system operates at LCoE levels still above those of large scale floating turbines. This gap mainly reflects differences in technology maturity, scale and operational efficiency, as AWE units currently lack both the economies of scale and the industrial optimisation achieved by the offshore wind sector.

Nevertheless, the sensitivity results show that investment driven cost reductions are a viable pathway to narrow this gap, especially in early deployment stages and highlight the importance of CapEx oriented policies for emerging offshore renewable technologies.

# 6 | Conclusions and Future Developments

This work presented a first techno economic assessment of offshore Airborne Wind Energy in the Italian maritime domain. By combining detailed offshore wind resource characterisation, a refined modelling approach for Annual Energy Production and an adapted techno-economic framework, the study offers new insights into the potential role of AWE in the Italian energy transition.

The wind analysis demonstrated that Mediterranean seas exhibits favourable high altitude wind regimes suitable for airborne operation. The study showed that wind speed increases significantly between 100 and 300 m and stabilises around 300–400 m, which aligns with the typical operating range of airborne systems, confirming that Italian offshore areas can provide the wind conditions required to support efficient AWE deployment.

Building upon the wind resource evaluation, it was developed a refined AEP model based on site specific Weibull parameters and the SkySails power curve. This approach replaces the idealised assumptions of previous conceptual models and yields more realistic estimates of Annual Energy Production under offshore Mediterranean conditions. The resulting producibility values fall within a technically credible range and are fully consistent with the high altitude wind resource observed in the Italian offshore domain.

The results confirm the capability of airborne systems to harness offshore winds with sufficient stability for energy generation. The comparison between ERA5 and CERRA also highlighted the importance of dataset resolution at elevated heights, whereas CERRA provides a more physically coherent description of the offshore atmosphere, which motivated its use as the reference dataset for the economic evaluation.

The techno-economic assessment provided the first estimate of the LCoE for an offshore AWE farm configured for the Italian context. In the absence of dedicated offshore cost models for airborne systems, the study extended the cost framework developed by Joshi et Al. by integrating floating wind cost components and adapting it to multi unit offshore deployment. The resulting LCoE reflects both the significant weight of the offshore

infrastructure and the early stage maturity of the AWE technology.

Several assumptions were necessary due to the limited availability of validated industrial data for airborne technologies. Under the assumptions adopted in this study, the resulting LCoE remains higher than that of mature offshore wind technologies. However, the sensitivity analysis showed that investment incentives and performance improvements can significantly reduce the LCoE, revealing clear pathways for potential cost reduction.

The results must be interpreted with caution because several phenomena that influence the real behaviour of an offshore plant could not be modelled. Wake interactions, turbulence intensity and aerodynamic coupling between neighbouring units remain open research challenges since no validated models or offshore measurements exist for multi unit airborne farms. Similarly, offshore cost elements were implemented using aggregated values that do not yet reflect the specific characteristics of airborne systems. These limitations underline the need for further technological development and more detailed data collection.

A first improvement concerns the spacing between AWE units within the farm and the estimation of wake losses and aerodynamic interactions between machines. Properly defining these distances is essential to avoid trajectory interference, reduce tether–tether collision risks and maintain stable crosswind flight patterns. A more accurate assessment of farm-level wake effects would also allow the optimisation of the layout, improving both energy yield and overall system reliability.

A second improvement concerns the definition of cost functions and the calculation of the LCoE, especially for offshore subsystems.In this study, offshore subsystem cost functions derived from conventional wind technology were applied; however, these models are calibrated for the scale of modern offshore wind farms, which have significantly larger installed capacities and different layout characteristics compared to current AWE systems. Developing cost functions specifically tailored to AWE would therefore improve the accuracy of future economic assessments and reduce the uncertainty associated with scaling traditional offshore costs to much smaller units.

A possible direction for future work is the extension of the COSMO-WF (Cost Model for Wind Farms) framework [18] to airborne systems. COSMO-WF is a well-established reference for offshore wind farms, since it parametrises each cost component using multiple physical and site-specific variables rather than only the farm size. Adapting this modelling philosophy to AWE could enable a more detailed and realistic representation of offshore cost drivers, moving beyond the aggregated expressions used in this thesis and allowing future optimisation studies based on component-level parametrisation.

As the technology evolves and becomes more mature, research in the field would naturally become more stable and aligned. Today, the absence of shared standards and reference protocols forces each study to adopt its own assumptions and modelling choices. The absence of standardised methods for deriving power curves, the small scale of current prototypes and the overall low technological maturity all contribute to greater uncertainty in existing analyses. Moreover, when it comes to sensitivity analyses and economic assessments, the lack of AWE specific references in official policy documents and renewable incentive schemes makes it harder to evaluate the realistic market entry of this technology.

Overall, the results of this thesis indicate that Airborne Wind Energy could become a valuable complement to conventional offshore wind. While challenges in technological maturity, regulation and cost competitiveness persist, the favorable high altitude wind resource and the structural simplicity of airborne systems justify continued research and early experimental deployment.

This work provides a coherent methodological foundation, region-specific wind analysis and the first techno-economic estimates for offshore AWES in Italy. Its findings may support future academic studies, inform policy development and guide early investment considerations as the technology advances toward commercial feasibility.

# Bibliography

[1] M. Alpino, L. Brugnara, M. G. Cassinis, L. Citino, F. David, A. Frigo, G. Papini, P. Recchia, and L. Sessa. Il recente sviluppo delle energie rinnovabili in italia. Technical Report 908, Banca d'Italia, Rome, Italy, 2025.

[2] R. M. Banta, Y. L. Pichugina, N. D. Kelley, R. M. Hardesty, and W. A. Brewer. Insight into wind properties in the turbine-rotor layer of the atmosphere from high-resolution doppler lidar. *Bulletin of the American Meteorological Society*, 94(6):883–902, 2013. doi: 10.1175/BAMS-D-11-00057.1.

[3] P. Bechtle, M. Schelbergen, R. Schmehl, U. Zillmann, and S. Watson. Airborne wind energy resource analysis. *Renewable Energy*, 141:1103–1116, 2019. doi: 10.1016/j.renene.2019.03.118.

[4] A. Candade. *Aero-structural Design and Optimisation of Tethered Composite Wings: Computational Methods for Initial Design of Airborne Wind Energy Systems*. PhD thesis, Delft University of Technology, 2023. URL `https://airbornewindeurope.org/wp-content/uploads/2023/12/tu-delft_Aero-structural-Design-and-Optimisation-of-Tethered-Composite-Wings_2023-12-06_compressed.pdf`.

[5] A. Cherubini, A. Papini, R. Vertechy, and M. Fontana. Airborne wind energy systems: A review of the technologies. *Renewable and Sustainable Energy Reviews*, 51:1461–1476, 2015. doi: 10.1016/j.rser.2015.07.053. URL `https://doi.org/10.1016/j.rser.2015.07.053`.

[6] Copernicus Climate Change Service. Copernicus regional reanalysis for europe (cerra). URL `https://climate.copernicus.eu/copernicus-regional-reanalysis-europe-cerra`.

[7] D. P. Dee, S. M. Uppala, A. J. Simmons, et al. The era-interim reanalysis: Configuration and performance of the data assimilation system. *Quarterly Journal of the Royal Meteorological Society*, 137(656):553–597, 2011. doi: 10.1002/qj.828.

[8] D. P. Dee et al. Reanalysis in climate monitoring. *Bulletin of the American Meteorological Society*, 95(8):1239–1248, 2014. doi: 10.1175/BAMS-D-13-00043.1.

[9] Gestore dei Servizi Energetici - GSE S.p.A. Avviso pubblico per la presentazione di domande a sportello per la concessione di contributi nell'ambito della missione 2, componente 2, investimento 1.2 del pnrr. Allegato 1 all'Avviso CACER 2025, July 2025. Finanziato dall'Unione Europea – NextGenerationEU.

[10] Q. Hassan, P. Viktor, T. J. Al-Musawi, B. M. Ali, S. Algburi, H. M. Alzoubi, A. K. Al-Jiboory, A. Z. Sameen, H. M. Salman, and M. Jaszczur. The renewable energy role in the global energy transformations. *Renewable Energy Focus*, 48:100545, 2024. doi: 10.1016/j.ref.2024.100545.

[11] H. Hersbach, B. Bell, P. Berrisford, et al. The era5 global reanalysis. *Quarterly Journal of the Royal Meteorological Society*, 146(730):1999–2049, 2020. doi: 10.1002/qj.3803.

[12] R. Joshi, D. Von Terzi, and R. Schmehl. System design and scaling trends in airborne wind energy demonstrated for a ground-generation concept. *Wind Energy Science*, 10(4):695–718, 2025. doi: 10.5194/wes-10-695-2025.

[13] S. Mann. An introduction to airborne wind: Technology and cost reduction trends, 2019. URL `https://ore.catapult.org.uk`. AP-0020.

[14] Ministero dell'Ambiente e della Sicurezza Energetica (MASE). Piano nazionale integrato per l'energia e il clima (pniec) 2021–2030. Technical report, Government of Italy, 2024. Updated English version, July 2024.

[15] A. Moino, A. Trebbi, N. Talia, G. Romano, and M. Sagretti. Lcairborne: A life cycle assessment of offshore airborne wind energy systems. Poster presented at the Airborne Wind Energy Conference (AWEC 2024), Madrid, Spain, 24–26 April 2024, 2024. URL `https://www.asp-poli.it/projects/lcairborne-2024`. Principal Academic Tutor: Prof. Alessandro Croce. Academic Tutors: Prof. Luca Sartori and Prof. Andrea Manzolini.

[16] E. Papadis and G. Tsatsaronis. Challenges in the decarbonization of the energy sector. *Energy*, 205:118025, 2020. doi: 10.1016/j.energy.2020.118025.

[17] M. Ridal, R. Randriamampianina, P. Dahlgren, et al. Cerra: The copernicus european regional reanalysis system. *Quarterly Journal of the Royal Meteorological Society*, 150:3385–3411, 2024. doi: 10.1002/qj.4664.

[18] M. X. A. Rodriguez. Design and implementation of a cost model for onshore and

offshore wind farms. Master's thesis, Politecnico di Milano, Milan, Italy, 2020. URL https://www.politesi.polimi.it/handle/10589/XXXXX. Supervisors: Prof. Alessandro Croce and Prof. Luca Sartori.

[19] M. X. A. Rodriguez. Design and implementation of a cost model for onshore and offshore wind farms. Master's thesis, Politecnico di Milano, Milan, Italy, October 2022. URL https://www.politesi.polimi.it/handle/10589/190690. Supervisor: Prof. Alessandro Croce. Co-supervisors: Prof. Luca Sartori and Eng. Marco Bianchini.

[20] L. A. C. Roque, L. T. Paiva, M. C. R. M. Fernandes, D. B. M. M. Fontes, and F. A. C. C. Fontes. Layout optimization of an airborne wind energy farm for maximum power generation. *Energy Reports*, 6:165–171, 2020. doi: 10.1016/j.egyr.2019.08.037.

[21] Y. Sakagami, P. A. A. Santos, R. Haas, J. C. Passos, and F. F. Taves. Wind shear assessment using wind lidar profiler and sonic 3d anemometer for wind energy applications – preliminary results. In *Proceedings of the World Renewable Energy Congress*. Springer, 2015. doi: 10.1007/978-3-319-17777-9_80.

[22] R. Schmehl, editor. *Airborne Wind Energy: Advances in Technology Development and Research*. Springer Nature, Singapore, 2018. ISBN 978-981-10-1946-3. doi: 10.1007/978-981-10-1947-0. URL https://doi.org/10.1007/978-981-10-1947-0.

[23] H. Schmidt, G. de Vries, R. Renes, and R. Schmehl. The social acceptance of airborne wind energy: A literature review. *Energies*, 15(4):1384, 2022. doi: 10.3390/en15041384. URL https://doi.org/10.3390/en15041384.

[24] SkySails Power GmbH. Skysails power data sheet venyo pn-14 rev3, 2025. URL https://www.skysails-power.com. Technical data sheet, Version REV3.

[25] T. S.p.A. Annuario statistico 2022. Technical report, Terna S.p.A., Roma, Italia, 2023. URL https://download.terna.it/terna/ANNUARIO%20STATISTICO%202022_8dbd4774c25facd.pdf. Rapporto sul fabbisogno energetico nazionale.

[26] T. Stehly, P. Duffy, and D. M. Hernando. 2022 cost of wind energy review. Technical Report NREL/PR-5000-88335, National Renewable Energy Laboratory (NREL), Golden, CO, USA, December 2023. URL https://www.nrel.gov/docs/fy24osti/88335.pdf. Includes cost and LCoE estimates for land-based, fixed-bottom, and floating offshore wind power plants commissioned in 2022.

[27] F. Trevisi, C. Riboldi, and A. Croce. Refining the airborne wind energy system power equations with a vortex wake model. *Wind Energy Science*, 8:1639–1650, 2023. doi: 10.5194/wes-8-1639-2023. URL https://doi.org/10.5194/wes-8-1639-2023.

[28] S. Trombini, E. Pasta, and L. Fagiano. On the kite-platform interactions in offshore airborne wind energy systems: Frequency analysis and control approach. *European Control Conference (ECC)*, 2024. URL https://arxiv.org/abs/2401.05950.

[29] U.S. Department of Energy. Challenges and opportunities for airborne wind energy in the united states: Report to congress. Technical report, U.S. Department of Energy, Wind Energy Technologies Office (WETO), Washington, DC, 2021. Available at: https://powerpedia.energy.gov/wiki/File:DOE_Logo_Color.png.

[30] H. Vos, F. Lombardi, R. Joshi, R. Schmehl, and S. Pfenninger. The potential role of airborne and floating wind in the north sea region. *Environmental Research: Energy*, 1:025002, 2024. doi: 10.1088/2753-3751/ad3fbc.

[31] J. Weber, M. Marquis, A. Cooperman, C. Draxl, R. Hammond, J. Jonkman, A. Lemke, A. Lopez, R. Mudafort, M. Optis, O. Roberts, and M. Shields. Airborne wind energy. Technical Report NREL/TP-5000-79992, National Renewable Energy Laboratory (NREL), Golden, CO, 2021. URL https://www.nrel.gov/docs/fy21osti/79992.pdf.

[32] J. Wei, T. Jiang, P. Ménager, D.-G. Kim, and W. Dong. Cop29: Progresses and challenges to global efforts on the climate crisis. *The Innovation*, 6(1):100748, 2025. doi: 10.1016/j.xinn.2024.100748.

# List of Figures

# List of Tables

# List of Symbols

## Latin Symbols

$a$ Weibull scale parameter

$AEP$ Annual Energy Production

$\overline{AEP}_{cell}$ Average AEP per grid cell

$AEP_{total}$ Total AEP of the Italian offshore domain

$CapEx$ Capital Expenditure

$CF$ Capacity Factor

$d$ Tether diameter

$E_k$ Energy produced in wind speed bin $k$

$f(v)$ Probability density function (Weibull)

$f_k$ Relative frequency of wind speed bin $k$

$H_k$ Equivalent annual hours for bin $k$

$k$ Weibull shape parameter

$L$ Tether length

$LCoE$ Levelized Cost of Energy

$n$, $N$ Number of observations / Total number of items

$n_{AWE}$ Number of AWE units per cell/farm

$OpEx$ Operational Expenditure

$P(v)$ Power output at wind speed $v$

$\overline{P}$ Average expected power output

$P_{farm}$ Total installed capacity of the farm

$P_{unit}$ Rated power of a single AWE unit

$r$ Pearson correlation coefficient

$r$ Real discount rate

$RMSE$ Root Mean Square Error

$Subsidy$ Financial incentive/grant

$T$ Project lifetime

$u$ East-West wind component

$v$ Wind speed

$\overline{v}$ Mean wind speed

$v_{cut-in}$ Cut-in wind speed

$v_{cut-out}$ Cut-out wind speed

$v_y$ North-South wind component

$z$ Vertical coordinate / Height above ground

## Greek Symbols

$\alpha$ Power law shear exponent

$\sigma$ Standard deviation of wind speed

## Acronyms and Abbreviations

**AEP** Annual Energy Production

**AWE** Airborne Wind Energy

**AWES** Airborne Wind Energy System

**BoP** Balance of Plant

**BoS** Balance of System

**CERRA** Copernicus European Regional Reanalysis

**ECMWF** European Centre for Medium-Range Weather Forecasts

**EEZ** Exclusive Economic Zone

**ERA5** ECMWF Reanalysis v5

**FG** Fly-Gen (Onboard Generation)

**GG** Ground-Gen (Ground Generation)

**ICC** Initial Capital Cost

**IEC** International Electrotechnical Commission

**LCOE** Levelized Cost of Energy

**OMC** Operations and Maintenance Costs

**PNIEC** Piano Nazionale Integrato per l'Energia e il Clima

**TRL** Technology Readiness Level

# Acknowledgements - Ringraziamenti

Desideriamo innanzitutto ringraziare il nostro relatore, il Professor Alessandro Croce, per averci dato la possibilità di svolgere questo lavoro di tesi. La ringraziamo per la passione che ci ha trasmessmo nella ricerca nel campo degli Airborne Wind Energy, per il supporto e per il costante stimolo durante tutto questo percorso.